Chemical Engineering Science 286 (2024) 119682

Contents lists available at ScienceDirect

Chemical Engineering Science

journal homepage: www.elsevier.com/locate/ces

Highly efficient lithium extraction from magnesium-rich brines with ionic liquid-based collaborative extractants: Thermodynamics and molecular insights

Gangqiang Yu [a,b], Xinhe Zhang [a], Tobias Hubach [b], Biaohua Chen [a,*], Christoph Held [b,*]

[a] Faculty of Environment and Life, Beijing University of Technology, 100 Ping Le Yuan, Chaoyang District, Beijing 100124, China
[b] Laboratory of Thermodynamics, Department of Biochemical and Chemical Engineering, TU Dortmund University, Emil–Figge–Str. 70, 44227 Dortmund, Germany

ARTICLE INFO

Keywords:
Extraction of lithium
Ionic liquid
ePC-SAFT
Quantum chemical calculation
Molecular mechanism

ABSTRACT

Selective extraction of Li^+ from high Mg^{2+}/Li^+ ratio brines with ionic liquid (IL) based collaborative extractants was investigated by experiments, thermodynamic analyses, and quantum chemical (QC) calculations. Effects of different IL cationic structures and organophosphorus ligands on extraction performances were studied. The results demonstrated that the system 1-(2-hydroxyethyl)-3-methylimidazolium bis(trifluoromethylsulfonyl) imide + trioctyl phosphate ([HOEMIM][Tf_2N] + TOP) was considered as the best extractant, with the very high extraction efficiency of Li^+ (83.16 %) and separation selectivity of Li^+/Mg^{2+} (742.11), which is higher than values reported in literature. The thermodynamic model ePC-SAFT was first extended to quantitatively predict the phase equilibria of the so-called "organic–inorganic complex strong electrolyte system" presented in this work. The molecular-level extraction mechanism was explored by QC calculation, indicating that the strong multi-site intermolecular interactions between Li^+ and [HOEMIM][Tf_2N] + TOP break the Li^+ hydration. This work provides guidance to rationally design novel IL-based extractants for efficient extraction of Li^+.

1. Introduction

Lithium (Li) as a strategy resource, has been widely applied in the various fields of lithium-ion batteries, aerospace, nuclear energy, medicine and ceramics due to its unique physicochemical properties (Su et al., 2022; Tarascon, 2010; Zhou et al., 2021). In response to the fossil energy crisis, electric vehicles are being developed more and more rapidly around the world, which leads to an unprecedently increase in the demand for lithium resources (Weil et al., 2009; Zhang et al., 2018; Zhou et al., 2019). Li resources mainly exist in hard rocks and salt lake brines, and the latter accounts for over 70 % of Li reserves worldwide (Choubey et al., 2016; Kesler et al., 2012). Currently, more than half of the Li_2CO_3 equivalents are obtained from salt lake brines because its cost of preparation is lower than that of extracting Li_2CO_3 from hard rock, as the brine is in a liquid state, allowing for a shorter process route (Kuang et al., 2018; Shi et al., 2018). The greatest challenge in extracting Li^+ from brines lies in the selective separation of Li^+/Mg^{2+} since Mg^{2+} is always accompanied by Li^+, often in greater amounts than Li^+, and to be separated in an efficient and economical manner. Furthermore, the Mg^{2+}/Li^+ ratio is a crucial factor in determining the feasibility and approach to Li^+ extraction from brines. Generally, South American brines have a relatively lower Mg^{2+}/Li^+ ratio, allowing for the relatively simple and low-cost precipitation method of Li extraction, despite with some inherent drawbacks. Mg^{2+}/Li^+ ratios are relatively high in most brines in China and in some brines in North America, and thus, it is a worldwide challenge to selectively extract Li^+ from the high Mg^{2+}/Li^+ ratio brines (Zhao et al., 2013).

Over the past decades, there are several methods for extracting lithium from brines, e.g., solvent extraction (Shi et al., 2020; Su et al., 2020; Zhou et al., 2012), precipitation (Li et al., 2015; Liu et al., 2018), adsorption (Gu et al., 2018; Jin et al., 2021), membrane separation (Li et al., 2019a; Xu et al., 2021) and electrochemical methods (Zhao et al., 2019). Among them, solvent extraction is the most promising for industrial applications due to its high extraction efficiency of Li^+, high separation selectivity of Li^+/Mg^{2+}, simple operation, low cost (Keller et al., 2021; Shi et al., 2019). In terms of solvent extraction, the extractants mainly used are β-diketones, crown ethers and organophosphorus. β-Diketones are usually used together with organophosphorus as a synergist extractant (Li and Binnemans, 2020), and suitable for separation Li^+/Na^+ instead of Li^+/Mg^{2+} (Wang et al., 2019; Zhang

* Corresponding authors.
E-mail addresses: chenbh@bjut.edu.cn (B. Chen), christoph.held@tu-dortmund.de (C. Held).

https://doi.org/10.1016/j.ces.2023.119682
Received 2 November 2023; Received in revised form 19 December 2023; Accepted 23 December 2023
Available online 25 December 2023

et al., 2021). Crown ethers are expensive due to the complex synthesis, which are usually used for separation of lithium isotopes (Li^6/Li^7), but not suitable for Li^+ extraction from bines (Cui et al., 2021). It is worth noting that organophosphorus ligands like tributyl phosphate (TBP), trioctylphosphine oxide (TOPO), triisobutyl phosphate (TIBP), and trioctyl phosphate (TOP), are usually considered as a kind of more suitable extractants for Li^+ extraction from high Mg^{2+}/Li^+ ratio brines (Pramanik et al., 2020; Yu et al., 2021b; Yu et al., 2019b). Particularly, TBP as one of the most representative organophosphorus extractants, is usually used in combination with $FeCl_3$ as a co-extractant as well as volatile organic solvents such as dichloromethane, dichloroethane, methyl isobutyl ketone, and kerosene as diluents. However, this inevitably results in the loss of volatile solvents and harm to the environment (Shi et al., 2020; Sun et al., 2023) Furthermore, the addition of $FeCl_3$ leads to the easy formation of a third phase in the extraction system (Zhou et al., 2012) which hinders mass transfer and is not conducive to continuously industrial processes. It is urgently required to develop and search a new class of co-extractants to replace $FeCl_3$ to form diluent-free extraction systems for efficient Li^+ extraction from high Mg^{2+}/Li^+ ratio brines.

Ionic liquids (ILs) as a new type of green solvents and materials have been widely studied in the fields of material synthesis (Chen et al., 2020), chemical reaction (Chen et al., 2011), extractive distillation (Lei et al., 2014), gas separation and absorption (Yu et al., 2021a; Yu et al., 2023; Yu et al., 2020; Yu et al., 2019a) liquid–liquid extraction like extraction of valuable chemicals (Jiang et al., 2021; Qin et al., 2016), aromatics extraction (Navarro et al., 2023; Song et al., 2016), extractive desulfurization (Song et al., 2015), and extractive denitrification (Chen et al., 2014), and extraction of metal ions (Cai et al., 2021; Li et al., 2019b; Zheng et al., 2021), owning to their unique characteristics like negligible vapor pressure, good hydrolysis and thermal stabilities, flammability, and tunable structures. Especially, ILs as extractants can be tuned through the design of cations and anions to improve the extraction efficiency and the selectivity of metal ions (Dupont and Binnemans, 2015; Li et al., 2021; Wang et al., 2017), For example, Rout and Binnemans have studied the solvent extraction of neodymium(III) from nitric acid medium by neutral extractant Cyanex 923 mixed with $[Tf_2N]^-$-based ILs. They showed that the extraction efficiency can be related to the solubility of the ILs cation in the aqueous phase (Rout and Binnemans, 2015), So far, the reports regarding the extraction of Li^+ using ILs as co-extractants are relatively rare from high Mg^{2+}/Li^+ ratio brines especially. The extraction efficiency of Li^+ with TBP combing with ILs ($[PF_6]^-$ and $[Tf_2N]^-$ as anions) as mixed extractants was investigated, and it is proved that the extraction mechanism of Li^+ follows the cation exchange, and the IL anion replaced $FeCl_4^-$ in the traditional TBP-$FeCl_3$ system to form a complex with Li^+ and TBP (Shi et al., 2014; Shi et al., 2016; Shi et al., 2017). The researcher synthesized $[BMIM]_3[PW_2O_{40}]$ to achieve a highly selective extraction of Li^+ from the high Mg^{2+}/Li^+ ratio brine, and the single-stage extraction efficiency of Li^+ reached 69.18 % under the optimal conditions (Wang et al., 2018). A comparative study on the extraction effect of Li^+ with different ILs based on C923 as a neutral ligand was achieved (Cui et al., 2019). However, the above-mentioned studies focus mainly on the experimental performances of the extraction of Li^+, and there are relatively few studies on extraction mechanisms. Particularly, there is a lack of systematic understanding on the effect of the structure of ILs on the extraction performance, as well as the thermodynamic behaviors during the extraction process. Even there is almost no research on unraveling the essential characteristics (intermolecular interactions) for separation mechanism of Li^+/Mg^{2+} at the molecular level related to IL-based extractants. These are crucial for the development and design of new IL-based extractants for highly efficient Li^+/Mg^{2+} separation. Furthermore, trial-and-error experimental measurements to obtain Li^+/Mg^{2+} separation performances are very time-consuming. Thus, it is needed to resort to molecular thermodynamic models, which can predict thermodynamic equilibria required for Li^+ extraction based on the molecular structures of components in mixed systems. This will further provide a thermodynamic property method to build the equilibrium stage and non-equilibrium stage models in the continuous industrial-scale Li^+ extraction process simulation and design. To the best our knowledge, there are no studies on the thermodynamic modelling of IL-related Li^+ extraction systems, due to the complexity of this system, and we refer to this system as "organic–inorganic complex strong electrolyte system". Thus, the ePC-SAFT equation of state (Cameretti et al., 2005) will be employed to describe the thermodynamic phase behavior for Li^+ extraction from bines with ILs.

In this work, we selected an aqueous solution of high Mg^{2+}/Li^+ molar ratio of 40:1 formulated with $MgCl_2$ and LiCl as the model brine as referred by the previous research (Li and Binnemans, 2021; Shi et al., 2016; Yu et al., 2019b), four $[Tf_2N]^-$-based ILs, and five organophosphorus ligands (corresponding structures and abbreviations are shown in Fig. 1). This work focuses on addressing the following issues: (i) identifying structure–property relationships between ILs (i.e., different cations) and organophosphorus ligand structures and extraction performance of Li^+ (extraction efficiency of Li^+ and separation selectivity of Li^+/Mg^{2+}) to determine the best IL-based extractants; (ii) exploring coordination mechanisms for Li^+ extraction by experimental coupled the advanced spectroscopy techniques; (iii) determining whether ePC-SAFT can be extended to predict the so-called phase equilibria of organic–inorganic complex strong electrolyte systems, and analyzing the thermodynamic properties (i.e., Gibbs free energy, enthalpy, and entropic changes) of the extraction process; (iv) revealing the molecular-level mechanism of Li^+/Mg^{2+} separation with IL-based extractants by analyzing binding energies, electrostatic potential (ESP) on molecular van der Waals (vdW) surfaces, and independent gradient models (IGM) based on quantum chemical (QC) calculations; and (v) investigating the washing and stripping performances of Li^+-rich organic phase, and recycling performance of collaborative extractants. This work provides a systematic understanding of IL-based extractants for Li extraction at the multiscale perspectives ranging from microscopic molecular mechanisms, thermodynamics and to extraction processes, aiming to provide theoretical guidance for developing and designing the novel IL-based extraction systems for high-efficiency Li^+/Mg^{2+} separation.

2. Experimental sections

2.1. Chemicals

LiCl (>99 wt%), $MgCl_2$ (>99 wt%), NaCl (99 wt%), NaOH and HCl were purchased from Beijing Enokai Technology Co., Ltd., China. Organophosphorus ligands, Cyanex 923 (C923), dibutyl phosphate (DBP), di-(2-ethylhexyl)phosphoric acid (P204), tributyl phosphate (TBP) and trioctyl phosphate (TOP) were obtained from Shanghai Bide Medical Technology Co., Ltd., China. ILs, 1-ethyl-3-methylimidazolium bis(trifluoromethylsulfonyl)imide ([EMIM][Tf_2N]), 1-butyl-3-methylimidazolium bis(trifluoromethylsulfonyl)imide ([BMIM][Tf_2N]), 1-octyl-3-methylimidazolium bis(trifluoromethylsulfonyl)imide ([OMIM][Tf_2N]), 1-(2-hydroxyethyl)-3-methylimidazolium bis(trifluoromethyl sulfonyl)imide ([HOEMIM][Tf_2N]) and 1-butylpyridinium bis (trifluoromethyl-sulfonyl)imide ([BPy][Tf_2N]) were purchased from Shanghai Chengjie Chemical Co.,Ltd., China.

2.2. Extraction experiments

All extraction experiments were carried out in a centrifuge tube of 50 mL. First, simulated brine (Li^+: 0.766 g/L, Mg^{2+}: 98.984 g/L, the high Mg^{2+}/Li^+ molar ratio of 40:1) was prepared by ultra-pure water as the aqueous phase. Then, a certain amount of IL was added to organophosphorus ligands to prepare the organic phase as an extractant system. The aqueous phase of 5 mL was taken and mixed with the organic phase at the given volume ratio. The mixture was shaken and subjected to centrifugal extraction at 300 r/min for 30 min to achieve extraction equilibrium. Subsequently, it was centrifuged at 8000 r/min for 5 min to

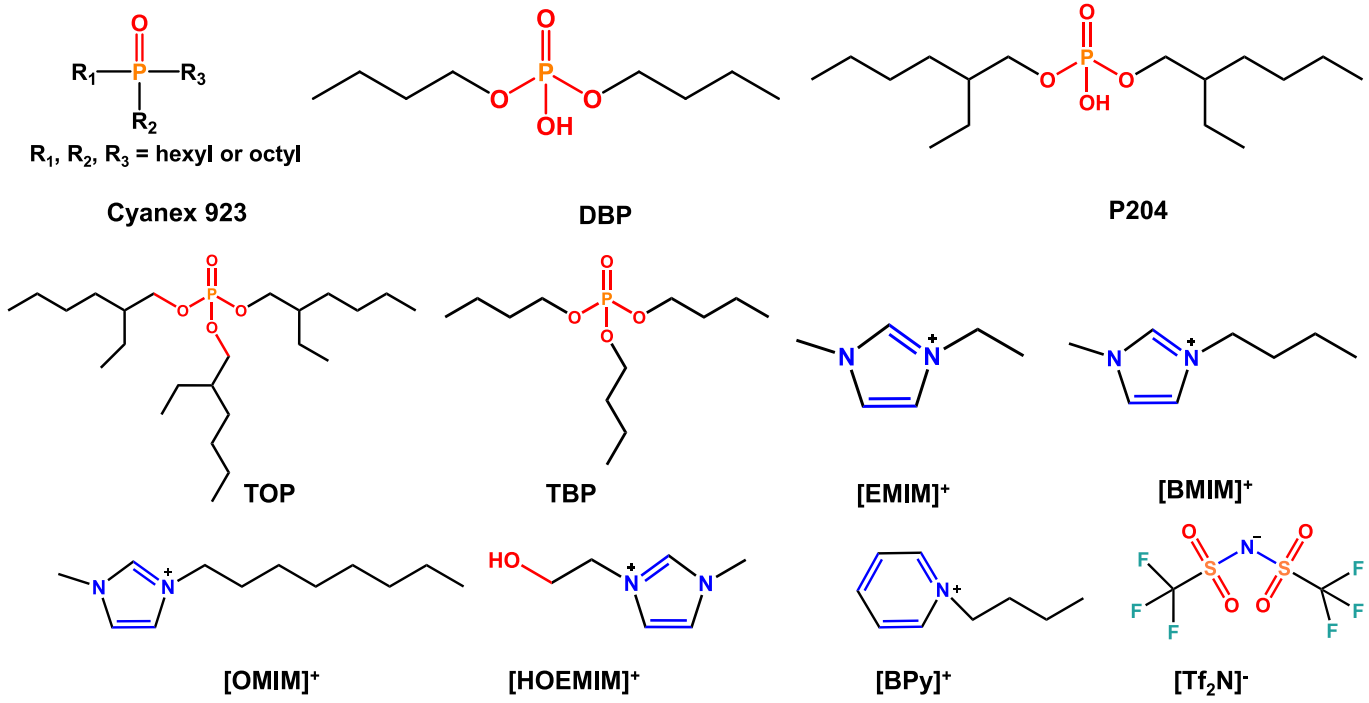

Fig. 1. Structures and abbreviations for organophosphorus ligands, cations and anions of ILs used in this work.

attain complete separation of the aqueous and organic phases. The concentrations of metal ions in the aqueous phase before and after extraction were measured by the inductively coupled plasma emission spectrometer (ICP-OES Optima 8000). The extraction efficiency (E_i) of metal ions, the distribution coefficient (D_i) of metal ions between the aqueous and organic phases, as well as the separation selectivity of Li^+/Mg^{2+} ($\beta_{Li^+/Mg^{2+}}$), were determined by the following relation:

$$E_i = \frac{C_0 - C_1}{C_0} \times 100\% \tag{1}$$

$$D_i = \frac{C_0 - C_1}{C_0} \times (V_A/V_O) \tag{2}$$

$$\beta_{Li+/Mg^{2+}} = \frac{D_{Li^+}}{D_{Mg^{2+}}} \tag{3}$$

Where C_0 and C_1 represents the concentration of given metal ions in the aqueous phase before and after extraction measured experimentally, respectively. V_A and V_O represent the volume of the aqueous and organic phases, respectively.

2.3. Measurements and characterization

The concentration for cation of ILs in aqueous phase was evaluated on the UV–visible spectroscopic (SHIMADZU UV-2600, Japan) to measure the number of cations involved in the reaction. The change of pH value in the aqueous phase was monitored via a pH meter (type SN B27310, Thermo Fisher Scientific Inc.) with an accuracy of 0.01. FTIR spectrometer (Spectrum Two™ FTIR Spectrometers, PerkinElmer) and ^{1}H NMR spectra (Bruker AVANCE HD III) were used to analyze the organic phase after and before extraction.

3. Thermodynamic modeling and theoretical calculations

3.1. ePC-SAFT model

The ePC-SAFT framework (Cameretti et al., 2005) used in this work calculates the residual Helmholtz energy (a^{res}) by incorporating various Helmholtz energy contributions. It extends the classical PC-SAFT model developed by Gross and Sadowski (Gross and Sadowski, 2001) which considers dispersive perturbations (represented by the contribution a^{disp}) and associating perturbations (represented by the contribution a^{assoc}) of a hard-chain reference fluid (described by a^{hc}). Additionally, ePC-SAFT considers the contribution of electrostatic interactions through the Debye-Hückel theory (Bülow et al., 2021a,b), namely the Helmholtz energy contribution a^{DH}.

$$a^{res} = a^{hc} + a^{disp} + a^{assoc} + a^{DH}(\varepsilon_r(x)) \tag{4}$$

Eq. (4) will be further denoted ePC-SAFT in this work. The dielectric constant $\varepsilon_r(x)$ of the medium is utilized in the calculation of a^{DH}. The

Table 1
Dielectric constants for all components applied in this work.

Component	Dielectric constant/C Vm^{-1}	Ref.
Water	$-105.2\ln(T[K]) + 677.480$	(Ascani and Held, 2021)
TOP	11	Set to constant number in this work
[HOEMIM][Tf_2N]	11	a)
Li^+	8	b)
Mg^{2+}	8	b)
Cl^-	8	b)

For the IL [HOEMIM][Tf_2N], a relative dielectric constant of 11 was chosen according to a previous work (Bülow et al., 2019).
All salts were modeled with a similar dielectric constant that is a mean of available experimental data (Andeen et al., 1970).

required pure-component values $\varepsilon_{r,j}$ for the solvents and ions used in the calculation are summarized in Table 1 (Andeen et al., 1970; Ascani and Held, 2021; Bülow et al., 2019). All ions were assigned the same value of $\varepsilon_{r,ion} = 8$. The dielectric constant of the medium $\varepsilon_r(x)$ was then calculated from a linear combination in the solvent mass fraction and the ion mole fraction:

$$\varepsilon_r(x) = \left(\sum_{j=1}^{N^{solv}} \varepsilon_{r,j} w_j^{solv}\right) x_{solv} + \sum_{j=1}^{N^{ion}} \varepsilon_{r,j} w_j^{ion} \tag{5}$$

In this equation, N^{solv} expresses the total number of components in the salt-free solvent mixture and N^{ion} the total number of ions. x_j and w_j denote the mole fraction and the mass fraction of component j. w_j^{solv} is the mass fraction of solvent j in the salt-free solvent mixture, while x_{solv} is the sum of the mole fraction of all solvents in the overall mixture. Associating components such as water are assigned five pure-component parameters, namely the segment number m_i^{seg}, segment diameter σ_{i}, dispersion-energy parameter u_i/k_{b} association-energy parameter $\varepsilon^{A_iB_i}/k_b$, and association-volume parameter $\kappa^{A_iB_i}$. For the ions considered in this work, two pure-component parameters, m_i^{seg} and σ_{i}, are utilized. Additionally, the 2B association scheme is used for water, TOP, IL and Li^+ during calculating associating interactions (Cameretti and Sadowski, 2008). Table 2 presents the pure-component parameters employed in this study (Held et al., 2008; Held et al., 2014).

The modeling of mixtures necessitates the utilization of the Berthelot-Lorentz (Berthelot, 1898; Lorentz, 1881) and Wolbach-Sandler (Wolbach and Sandler, 1997) combining rules:

$$\sigma_{ij} = \frac{1}{2}(\sigma_i + \sigma_j) \tag{6}$$

$$u_{ij} = \sqrt{u_i u_j (1 - k_{ij})} \tag{7}$$

$$\varepsilon^{A_iB_j} = \frac{1}{2}(\varepsilon^{A_iB_i} + \varepsilon^{A_jB_j})(1 - k_{ij}^{hb}) \tag{8}$$

$$\kappa^{A_iB_j} = \sqrt{\kappa^{A_iB_i}\kappa^{A_jB_j}} \left(\frac{\sqrt{\sigma_i\sigma_j}}{1/2(\sigma_i + \sigma_j)}\right)^3 \tag{9}$$

In Eq. (8), the binary interaction parameter k_{ij} is introduced, allowing for the modification of the dispersion energy of the pair ij. Binary interaction parameters were required for the following pairs: ion-ion, ion-water, ion-TOP and TOP-water. Particularly, the ePC-SAFT model has been shown to be predictive for phase equilibria in complex mixtures of up to 6 components (Ascani et al., 2022). That is, fit parameters usually have not to be adjusted to the multicomponent mixture of interest, but only to the subsystems. The parameter for the IL-water pair was fitted to the phase equilibrium between IL and water, while the remaining parameters were fitted to one experimental data point. In addition, the binary interaction parameter k_{ij}^{hb} for the association parameter of mixtures for the TOP-Li^+ system was adjusted to account for the coordination of Li^+ to the P═O group of TOP. The binary interaction parameters used in this study are listed in Table 3 (Chapeaux et al., 2007; Held et al., 2014). For Mg^{2+} binary interaction parameters were not applied. In this study, we found that only one fit parameter was required to match the data quantitatively correct (Li^+-TOP, see Table 3), while other interaction parameters were not used or were used to switch off the dispersion interaction (i.e., value equal to one, see Table 3), or fitted to the subsystem (e.g., Li^+-Cl^-, or water-IL).

Table 3
Binary interaction parameters k_{ij} used in this work.

Parameters	k_{ij}	k_{ij}^{hb}
Water – [HOEMIM][Tf_2N]	0.007[a)]	–
Li+ – TOP	0.3	0.3
Water – TOP	1	–
Li^+ – [HOEMIM][Tf_2N]$^-$	1	1
Li^+ – Water	–	1
Li^+ – Cl^-	0.669 from reference (Held et al., 2014)	–

a) Fitted to binary data water- [HOEMIM][Tf_2N] from the reference (Chapeaux et al., 2007).

3.2. Quantum chemical (QC) calculations

The quantum chemical (QC) calculation based on the density function theory (DFT) was performed to identify the molecular-level extraction separation mechanism. The initial geometrical configurations regarding metal ion hydrates, IL, TOP, and the complex of metal ions and IL/TOP were optimized by the Gaussian 09 program (Version D.01) (Frisch et al., 2009) at the B3LYP/6–31 + G(d, p) level (M. et al., 2005), with the DFT-D3(BJ) dispersion correction (Grimme et al., 2011). The frequency calculation was carried out to ensure the stability of the obtained geometry with the lowest energy. Based on the above configuration, the binding energies of complexes ($\Delta E_{\text{Complex}}$) between clusters were calculated by:

$$\Delta E_{\text{Complex}} = E_{A-B} - E_A - E_B \tag{10}$$

Where $E_{\text{A-B}}$, E_{A} and E_{B} represent the electron energy (in kcal/mol) of complexes of A-B, cluster A and cluster B, respectively. Moreover, the ESP analysis of molecular vdW surfaces and IGM analysis were performed by the Multiwfn tool (version 3.8) as developed by Lu and Chen (2012) to visually identify the type, strength and location of intermolecular interactions formed and to deeply explore extraction mechanism.

4. Results and discussion

4.1. Structural effects of ILs and organophosphorus ligands on extraction performance

The extraction performance for the five different structural organophosphorus ligands (i.e., C923, DBP, P204, TBP and TOP) containing the P═O group were experimentally measured and compared to explore the structure–property relationship under the specific IL [BMIM][Tf_2N] at the given operation conditions (e.g., molar ratio of Mg^{2+} to Li^+ in the aqueous phase Mg^{2+}/Li^+ = 40:1, the volume ratio for organic to aqueous phase O/A = 3:1, pH = 7, and IL concentration in organic phase C_{IL} = 0.1 mol/L), and the results are shown in Fig. 2 (see Table S1 in

Table 2
The ePC-SAFT pure-component parameters used in this work.

Component	m_i^{seg}	σ_{i} (Å)	u_i/k_{b} (K)	$\varepsilon^{A_iB_i}/k_b$ (K)	$\kappa^{A_iB_i}$	Association scheme	Refs
Water	1.2047	a)	353.95	2425.7	0.0451	2B	(Held et al., 2008)
TOP	4.2032	5.4506	280.4777	6393.5	0.0001	2B	This work
[HOEMIM][Tf_2N]	4.073	4.6432	434.6120	5000	0.1	2B	This work
Li^+	1	2.8449	360.00	0	100	2B	This work
Mg^{2+}	1	3.1327	1500	–	–	–	(Held et al., 2014)
Cl^-	1	2.7560	170.00	–	–	–	(Held et al., 2014)

a) $\sigma = 2.7927 + (10.11 \cdot e^{-0.01775T} - 1.417 \cdot e^{-0.01146T})$ with T in K.

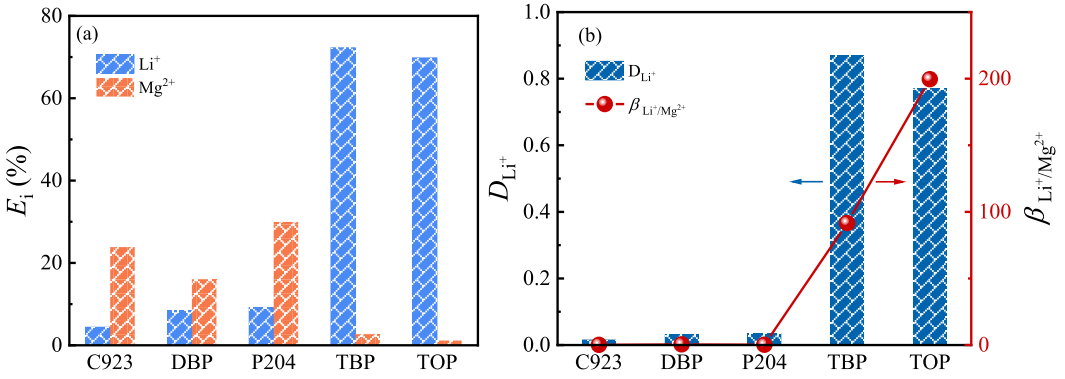

Fig. 2. Effects of different ligands on the extraction efficiency (a) and separation performances (D_{Li^+} and $\beta_{Li+/Mg^{2+}}$) of Li^+/Mg^{2+} (b) in the presence of [BMIM][Tf_2N] (molar ratio of Mg^{2+} to Li^+ in the aqueous phase $Mg^{2+}/Li^+ = 40:1$; the volume ratio for organic to aqueous phases O/A = 3:1; pH = 7; and IL concentration in organic phase C_{IL} = 0.1 mol/L) at 298.15 K.

Supplementary material for more details). It can be seen form Fig. 2a that the Li^+ extraction efficiencies for ligands TBP (72.27 %) and TOP (69.81 %) are very close to each other, which are far higher than those for any of others. Meanwhile, the similar phenomenon is also presented in the distribution coefficients of Li^+ (Fig. 2b). Noteworthily, the separation selectivity of Li^+/Mg^{2+} of TOP is up to the highest 199.63 among all the ligands and much higher than that of TBP. This is because that TOP has the longer alkyl chains with the branch chains, which leads to greater steric hindrance to combine Mg^{2+} with larger radius. Therefore, TOP is a preferred candidate ligand to perform the experiment below in this work.

The structural effect of hydrophobic ILs containing different cations under the same anion $[Tf_2N]^-$ on the extraction performance of Li^+ with TOP as the ligand at the given operating conditions ($Mg^{2+}/Li^+ = 40:1$; O/A = 3:1; pH = 7 and C_{IL} = 0.1 mol/L), and the results are shown in Fig. 3 (see Table S2 in Supplementary material for more details). Fig. 3a shows that the extraction efficiency of Li^+ in different $[Tf_2N]^-$-based ILs follows the order of [OMIM][Tf_2N] (39.51 %) < [BMIM][Tf_2N] (69.6 %) < [EMIM][Tf_2N] (73.69 %), which evidently indicates that the IL with the longer alkyl chain is unfavorable for extracting Li^+ ions. This may be attributed to two reasons as follows: the longer alkyl chain to (i) increase the IL hydrophobicity resulting in weakening the exchange capacity with Li^+, and (ii) increase the IL viscosity leading to weaken the Li^+ mass transfer from aqueous to organic phases. It should be noted that the cationic structural effect on the extraction efficiency and distribution coefficient of Li^+ follows the order of [OMIM][Tf_2N] < [BMIM][Tf_2N] < [BPy][Tf_2N] < [EMIM][Tf_2N] < [HOEMIM][Tf_2N] (Fig. 3a). Generally, it seems to be not obvious for the cationic structural effect on the extraction performance of Mg^{2+}. This leads to the result that the cationic structural effect on the separation selectivity of Li^+/Mg^{2+} is similar to the effects on extraction efficiency and distribution coefficient of Li^+ following the same trend (except for the inconsistent phenomenon of [BMIM][Tf_2N] > [BPy][Tf_2N]) (Fig. 3b). Thus, the cation with the shorter alkyl chain is preferred. Particularly, the extraction efficiency of Li^+ can be greatly enhanced from 73.69 % to 80.27 %, and separation selectivity of Li^+/Mg^{2+} much increased from 206.88 to 709.92 when a hydroxyl group is introduced into the alkyl chain of the cation of [EMIM][Tf_2N] to become [HOEMIM][Tf_2N]. This is resulted from the fact that the presence of hydroxyl group can intensify the affinity of cations to water, which made it easier to enter the aqueous phase for exchange with Li^+. Therefore, [HOEMIM][Tf_2N] is selected as the IL candidate for the subsequent study. Meanwhile, The IL [HOEMIM][Tf_2N] exhibits good thermal stability (the onset decomposition temperature is about 400 °C), and the relatively low viscosity (73 mPa·s at 30 °C) (see Fig. S1 in Supplementary material), which can be further decrease due to the presence of water during Li^+ extraction processes.

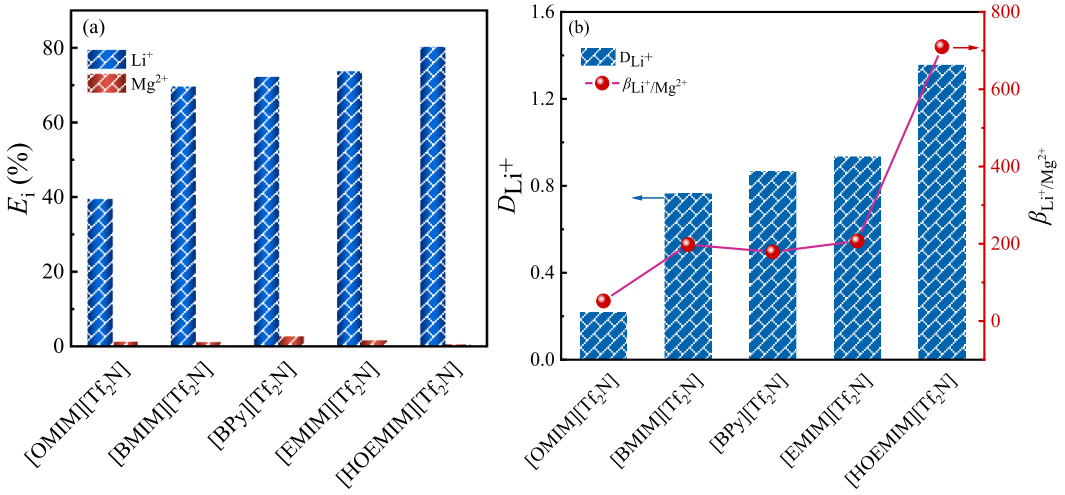

Fig. 3. Effects of different ILs on extraction efficiency (a) and separation performances (D_{Li^+} and $\beta_{Li+/Mg^{2+}}$) of Li^+/Mg^{2+} (b) with TOP as a neutral ligand ($Mg^{2+}/Li^+ = 40:1$; O/A = 3:1; pH = 7 and C_{IL} = 0.1 mol/L) at 298.15 K.

4.2. Optimizing operating conditions for extraction processes

The operating conditions (i.e., pH values, IL concentration C_{IL}, and O/A ratio) for extraction of Li^+ were optimized, and the results are shown in Fig. 4 (see Tables S3–S5 in Supplementary material for more details). As shown in Fig. 4a and b, when the pH value increased from 1 to 4, the extraction efficiency of Li^+ shows a slight upward trend from 75.82 % to 83.44 %, while there will be no significant change when the pH value is higher than 4. The extraction efficiency of Mg^{2+} has a slight decrease trend over the range from 1 to 7. When pH value is greater than 7, there are white $Mg(OH)_2$ precipitates from the aqueous phase, so the pH value has to be controlled to be within 7. The strong acidity environment is unbeneficial to extraction Li^+ process, which is attributed to the fact that the competitive effect between H^+ and Li^+ result in the lower separation selectivity of Li^+/Mg^{2+}. Particularly, the higher pH value is in favor of higher separation selectivity, which is due to gradually decreasing distribution coefficient of Mg^{2+} with increasing the pH value. Moreover, separation selectivity of Li^+/Mg^{2+} increases from 67.85 to 709.01 rapidly as the pH value rises from 4 to 7. Accordingly, the optimal pH value for the extraction system is 7.

The effect of IL concentration on the extraction performance is shown in Fig. 4c and d. It is found that using only TOP has almost no extraction ability for Li^+ and Mg^{2+}. When the [HOEMIM][Tf_2N] concentration increases from 0 to 0.09 mol/L, the extraction efficiency of Li^+ sharply increases with up to 80 % for the concentration of 0.09 mol/L. For IL concentrations greater than 0.09 mol/L, the extraction efficiency of Li^+ remains almost a constant. However, the separation selectivity of Li^+/Mg^{2+} decreases for IL concentrations greater than 0.09 mol/L. This is because of the fact that the saturated extraction of Li^+ will be reached under the IL concentration of 0.09 mol/L, which leads to an excess of IL increasing the ability to extract Mg^{2+} and elevating the distribution coefficient of Mg^{2+}. Therefore, the [HOEMIM][Tf_2N] concentration of 0.09 mol/L is selected an optimal value.

The effect of O/A ratios on the extraction performance are shown in Fig. 4e and f. It is found from Fig. 4e that when the O/A ratio increases from 1:1 to 3:1, the extraction efficiency of Li^+ presents an obvious upward trend. Subsequently, when the O/A ratio increases from 3:1 to 6:1, the increase in extraction efficiency of Li^+ tends to level off. Fig. 4f shows that separation selectivity of Li^+/Mg^{2+} increases significantly when the O/A ratio increases from 1:1 to 3:1, with a maximum value of 742.11, while it will decrease when the O/A ratio is increased to values greater than 3:1. This is because the extraction of Li^+ by IL + TOP reached saturation at this ratio, and continuing to increase the amount of IL + TOP enhanced the extraction capacity of Mg^{2+}. Thus, O/A ratio

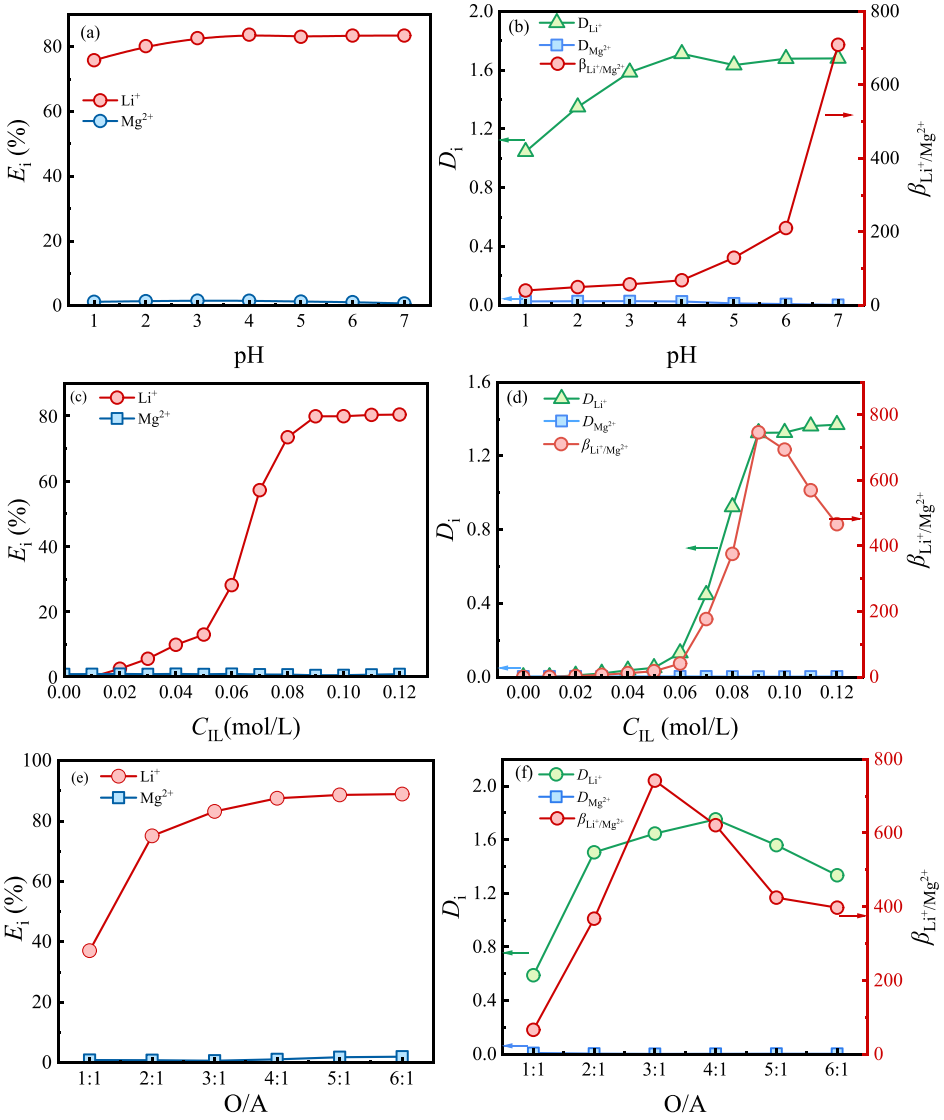

Fig. 4. Effects of pH values (a, b; $Mg^{2+}/Li^+ = 40:1$, O/A = 3:1 and C_{IL} = 0.1 mol/L), IL concentrations C_{IL} (c, d; $Mg^{2+}/Li^+ = 40:1$, O/A = 3:1 and pH = 7) and O/A ratios (e, f; $Mg^{2+}/Li^+ = 40:1$; and pH = 7 and C_{IL} = 0.09 mol/L) on extraction performances with [HOEMIM][Tf_2N] + TOP as extractant system at 298.15 K.

Table 4
Comparison of extraction performances of Li^+ with different extractant systems at 298.15 K.

Ligands	ILs	Mg^{2+}/Li^+ molar ratios	One-stage Li^+ extraction efficiency (%)	$\beta_{Li^+/Mg^{2+}}$	O/A	pH	Refs.
TBP	[HOEMIM][Tf_2N]	40	80	170	1:1	7	(Li and Binnemans, 2021)
TBP	[BMIM][PF_6]	12.58	90.93 (92.5)	- (–)	2:1(3:1)	7	(Shi et al., 2014)
TBP	[BMIM][Tf_2N]	13.05	92.37 (94.61)	403.33 (–)	2:1(3:1)	7	(Shi et al., 2016)
TBP	[BMIM]$_3PW_{12}O_{40}$	78.33	69.18 (72)	283.06 (210)	1:1(3:1)	7	(Wang et al., 2018)
TIBP	[EMIM][Tf_2N]	9.54	83.71 (91.66)	71.24 (138.61)	1:1(2.5:1)	7	(Gao et al., 2015)
TBP	[MMIM]$_4SiW_{12}O_{40}$	78.33	60 (65)	35 (125)	1:1(3:1)	7	(Wang et al., 2023)
TOP	[HOEMIM][Tf_2N]	40	83.16	742.11	3:1	7	This work

Note: The O/A in the brackets corresponds to the Li^+ extraction efficiency and $\beta_{Li^+/Mg^{2+}}$.

of 3:1 is a suitable selection. In addition, a comparison of extraction performance with different extractant systems collected from literature are shown in Table 4 (Gao et al., 2015; Li and Binnemans, 2021; Shi et al., 2014; Shi et al., 2016; Wang et al., 2023; Wang et al., 2018). It is found that the [HOEMIM][Tf_2N] + TOP extractant system in this work has the very highest max one-stage extraction efficiency of Li^+ (83.16), and separation selectivity of Mg^{2+}/Li^+ (742.11) is highest among all extractant systems collected from literature. Besides, when compared with the extractant systems of [HOEMIM][Tf_2N] + TBP, TBP-[BMIM]$_3PW_{12}O_{40}$ + TBP and [MMIM]$_4SiW_{12}O_{40}$, + TBP, the extraction performance using [HOEMIM][Tf_2N] + TOP is significantly improved. In summary, the extractant system of [HOEMIM][Tf_2N] + TOP proposed in this study had great selective extraction ability for Li^+.

The multistage extraction experiment was carried out to validate the extraction performance of Li^+ with the extractant of IL + TOP in the real industrial application at the above-mentioned optimized conditions, and the results are shown in Fig. S2 in Supplementary material. It can be seen that the extraction efficiency of Li^+ reached 99.07 %, and Li^+ concentration in the aqueous phase decreased from the original 760.6 mg/L to 7.1 mg/L after five stage extractions. The results show that the IL + TOP composition is a promising extractant applied for extraction of Li^+ from the brine with high Mg^{2+}/Li^+ ratio.

4.3. Analyses of extraction mechanisms via spectroscopy techniques

4.3.1. Analyses of ^1H NMR, UV–visible, and FTIR

Fig. 5a and b show that the ^1H NMR spectra of the organic phase does not change significantly before and after extraction. The chemical shift corresponding to the hydroxyl peak of $[HOEMIM]^+$ at 3.81 ppm, and the peak intensity is weakened after extraction, indicating that $[HOEMIM]^+$ may be exchanged into the aqueous phase, resulting in a decrease in $[HOEMIM]^+$ concentration. In addition, the UV–visible spectrum was used to analyze the spectrum of raffinate (i.e., the aqueous phase) at 190 ~ 250 nm (see Fig. S3), there is an obvious absorbance peak of $[HOEMIM]^+$ presented at 209 nm. It is found that the cation $[HOEMIM]^+$ species in the aqueous phase after extraction are determined although when the metal ions are not added into the aqueous phase. This is due to the certain solubility of IL in the aqueous solution with the $[HOEMIM]^+$ concentration of 0.7135 g/L measured quantitatively. However, the absorbance strength of the aqueous phase with metal ions (the $[HOEMIM]^+$ concentration of 11.7477 g/L measured quantitatively) is significantly higher than that without metal ions. This completely the presence of metal ions in the aqueous phase can enhance the $[HOEMIM]^+$ entered from the oil phase into the aqueous phase, which is the significant evidence for occurring the cationic exchange mechanism. Fig. 5c showed the FTIR spectra of [HOEMIM][Tf_2N], TOP and their mixing. It is found that all peaks of [HOEMIM][Tf_2N] and TOP still existed after mixing, indicating that [HOEMIM] and TOP were physically mixed. Fig. 5d and e show the characteristic information of FTIR spectra for the organic phase before and after extraction, and the wavelengths at 2959 cm^{-1} and 2872 cm^{-1} corresponded to the asymmetric and symmetric tensile vibration of CH_3 group, respectively. Moreover, the peaks at 1463 cm^{-1} and 1380 cm^{-1} are assigned to the asymmetric and symmetric bending vibrations of CH_3 respectively, 1014 cm^{-1} is attributed to the tensile vibration of P-O-C, and all of these peaks are not shifted. However, the peak at 1269 cm^{-1} representing P═O in TOP is shifted to 1259 cm^{-1} after extraction. This is because that the P═O vibration frequency changed is resulted by combining TOP with Li^+, representing the strong interaction is formed between TOP with Li^+. The peaks at 1352 cm^{-1}, 1189 cm^{-1}, and 1051 cm^{-1} are corresponding to characteristic information of S═O, C-F, S-N-S in $[Tf_2N]^-$, respectively, and all of them have not obvious shift, indicating the anion of IL still stays in the organic phase after extraction instead of the aqueous phase. It is found from Fig. S4 in Supplementary material that the C═C stretching vibration in imidazolium ring on $[HOEMIM]^+$ at 1572 cm^{-1} disappeared after extraction, which is due to the ion exchange happened between $[HOEMIM]^+$ and Li^+ in the aqueous phase, resulting in the decrease of $[HOEMIM]^+$ concentration in organic phase. The results are in the agreement with those obtained by UV–visible and ^1H NMR spectra.

4.3.2. Extraction equilibrium parameters

According to the analyses of FTIR, ^1H NMR and UV–visible spectra, the extraction process can be treated as the following relation:

$$[HOEMIM][Tf_2N]_{org} + Li^+_{aq} + nTOP_{org} \rightarrow [HOEMIM]^+_{aq} + [Li{\cdot}nTOP]^+_{org} + [Tf_2N]^-_{org} \quad (11)$$

where subscripts "aq" and "org" represent the aqueous and organic phases respectively, and n represents the number of TOP molecules. The extraction equilibrium constant (K) can be expressed as:

$$K = \frac{D_{Li^+}\cdot[HOEMIM]^+_{aq}}{[HOEMIM]^+_{aq}[HOEMIM]^n_{org}}, D_{Li^+} = \frac{[Li{\cdot}nTOP]^+_{org}}{[Li]^+_{aq}} \quad (12)$$

Since, it can be further represented by as follows:

$$\log D_{Li^+} + \log[HOEMIM]^+_{aq} - \log[HOEMIM]^+_{org} = n\log[TOP]_{org} + \log K \quad (13)$$

The $n = 1$ was determined by calculating the slop of curve (see Fig. S5 in Supplementary material), indicating that one TOP molecule can bind with one Li^+.

4.4. Extraction thermodynamic behaviors

4.4.1. Phase equilibria behavior predicted by the ePC-SAFT model

In this study, phase equilibria were calculated using the isofugacity criterion, which states that at thermodynamic equilibrium, the fugacity of each component is equal in all phases.

$$f_i^1 = f_i^2 = \cdots = f_i^\pi \quad (14)$$

For calculation of the fugacities, the so-called "$\varphi - \varphi$" criterion was used. The fugacity of each component in both phases was expressed using the respective fugacity coefficient as below:

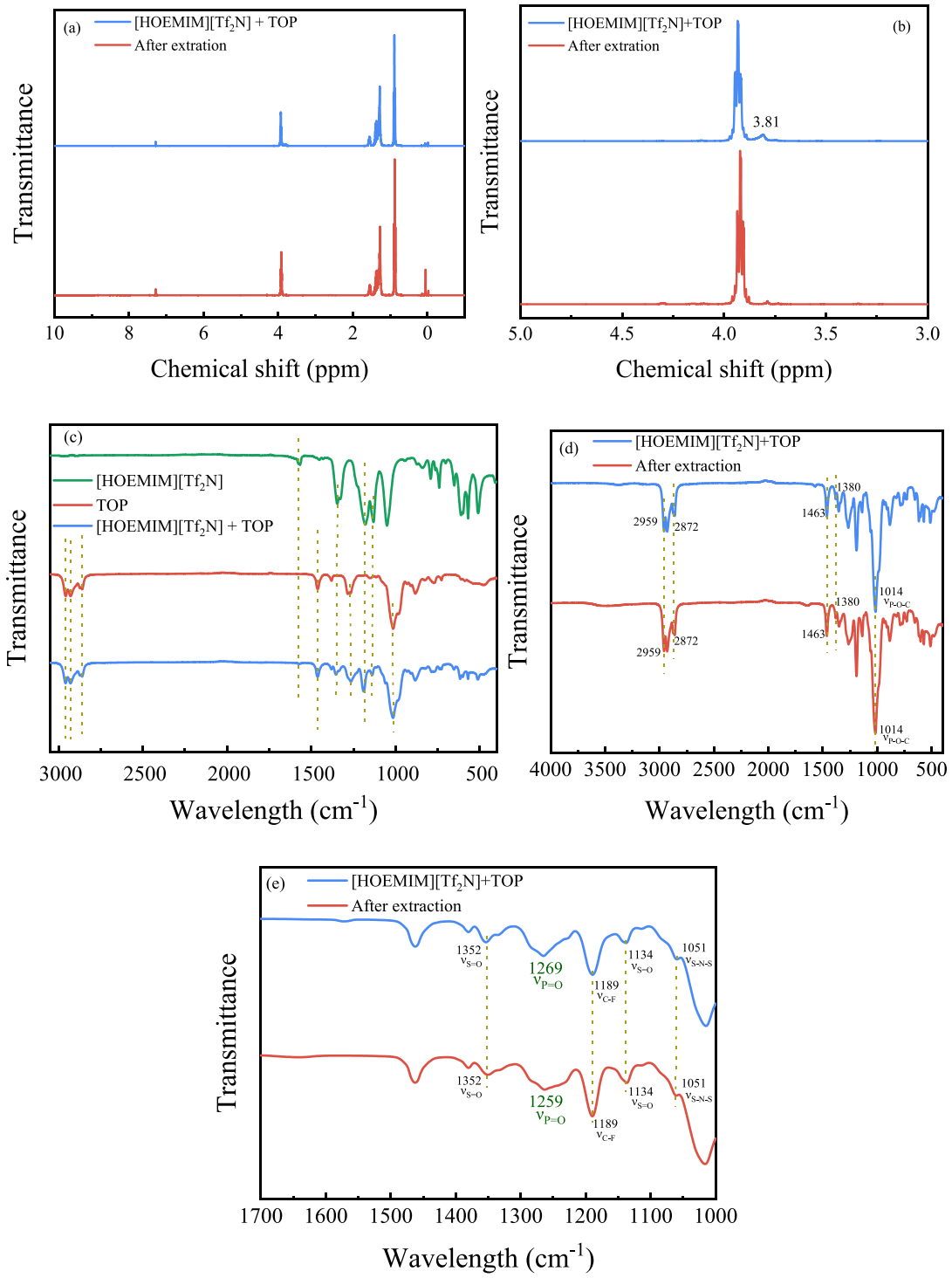

Fig. 5. ^{1}H NMR of (a, b; b is the partial magnification of a) and FTIR (c-e; e is the partial magnification of d) spectra for organic phase before and after extraction (10 v% IL + 90 v% TOP, and O/A = 3:1) at 298.15 K.

$$\varphi_i^{L1} x_i^{L1} = \varphi_i^{L2} x_i^{L2} \tag{15}$$

The fugacity coefficients φ_i can be derived with ePC-SAFT from the residual Helmholtz energy a^{res} via the chemical potential μ_i as expressed in Equation (16)

$$\ln(\varphi_i) = \frac{\mu_i^{res}}{k_B T} - \ln\left(1 + \left(\frac{\partial\left(\frac{a^{res}}{k_B T}\right)}{\partial \rho}\right)\right) \tag{16}$$

Therefore, with the phase equilibrium calculation, the extraction efficiency of Li^+ and Mg^{2+} were determined using:

$$E_i = \frac{\phi \cdot x_{i,\text{org,phase}}}{x_{i,\text{Feed}}} \tag{17}$$

where ϕ accounts for the molar ratio between the organic and aqueous phase.

The three binary parameters between Li^+ and TOP and between TOP and the IL were optimized to enhance the accuracy of the E_{Li+} data point

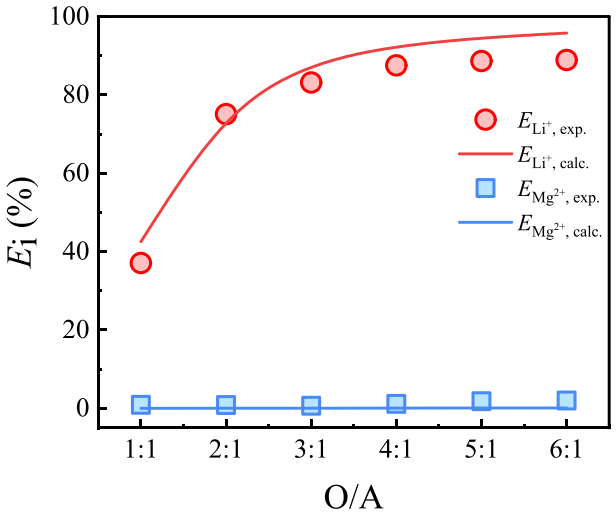

Fig. 6. Comparison of the calculated (lines) and experimental (points) on the effects of the volume ratio for the organic to aqueous phase (O/A) on Li^+ and Mg^{2+} extraction efficiency with [HOEMIM][Tf_2N] + TOP as extraction system ($Mg^{2+}/Li^+ = 40:1$; and pH = 7 and $C_{IL} = 0.09$ mol/L). ePC-SAFT parameters are taken from Tables 1–3, and the parameters were fitted to E_{Li+} at O/A = 2:1 and 298.15 K, i.e., all other modeling lines are predictions.

at O/A = 2:1. All the binary interaction parameters to Mg^{2+} were set to zero. Further, dispersion between water and TOP, as well as TOP and IL was not accounted for ($k_{ij} = 1$). Fig. 6 illustrates the modelled extraction efficiency for Li^+ and Mg^{2+} at various ratios between the organic and aqueous phases (see Table S6 in Supplementary material for more details). Not surprisingly, the ePC-SAFT modelling of E_{Li+} at O/A = 2:1 is in the quantitative agreement to the experimental data since this was the fitting point. Conversely, the calculations for the other O/A ratios are predictive. The results clearly demonstrate that a ratio O/A = 1:1 yields a notably lower extraction efficiency, which is captured by ePC-SAFT qualitatively. The ePC-SAFT overestimates the extraction efficiency at this ratio. Anyway, the prediction at ratios O/A > 1 agrees quantitatively with the experimental data. As the O/A ratios increase, E_{Li+} finally arrives at a limiting value of approximately 85 %. Additionally, the ePC-SAFT correctly predicts that the extraction efficiency of Mg^{2+} is negligible across all ratios. Remarkably, this behavior was obtained without the need to adjust additionally binary interaction parameters. Therefore, the ePC-SAFT model demonstrates the powerful prediction capacity and is first successfully extended to describe the so-called "organic–inorganic complex strong electrolyte system" in Li^+/Mg^{2+} extraction separation with ILs.

4.4.2. Analyses of Gibbs free energy, enthalpy and entropy

The thermodynamic analyses for Gibbs free energy (ΔG), enthalpy (ΔH) and entropy (ΔS) in the extraction process were investigated. As shown in Fig. 7a, both the extraction efficiency and distribution coefficient of Li^+ decrease with the increase in temperatures. Based on the Van't Hoff relation, the enthalpy change can be calculated by

$$\log K = \frac{\Delta H}{2.303RT} + C \tag{18}$$

where R is the universal gas constant, and C is the integral constant. Fig. 7b shows that the slope of the plot is $\Delta H/2.303R$, so the calculated ΔH is −10.33 kJ/mol, indicating the extraction of Li^+ is an exothermic process, and low temperature is beneficial to this process. ΔG and the ΔS can be also obtained by

$$\Delta G = -2.303RT \cdot \log K = \Delta H - T \cdot \Delta S \tag{19}$$

Consequently, the values of ΔG and ΔS are −0.90 kJ/mol and −31.65 J/K/mol, respectively, indicating that the extraction reaction is orderly spontaneous.

4.5. Molecular insights into extraction processes

4.5.1. Analysis of binding energy

It is very significant to identify the extraction mechanism at the molecular level for extraction separation of Li^+/Mg^{2+}. The binding energies of between Li^+/Mg^{2+} and H_2O, IL, and TOP were calculated by QC calculations, and the results are shown in Fig. 8. In the aqueous solution, Li^+ can be coordinated with four H_2O molecules, while Mg^{2+} can be coordinated with six H_2O molecules (Marcus, 1988; Olsher et al., 1991). By comparing Fig. 8b and e, it can be found that the binding energy of Mg^{2+}-$6H_2O$ (−337.41 kcal/mol) is much greater than that of Li^+-$4H_2O$ (−114.39 kcal/mol), indicating that Mg^{2+} has stronger hydration in the aqueous phase, which makes Mg^{2+} more difficult to extract from the aqueous phase than Li^+. As shown in Fig. 8A–C, the magnitude of interaction energy is in the order of Li^+-$[Tf_2N]^-$ (−133.09 kcal/mol) > Li^+-$4H_2O$ (−114.39 kcal/mol) > Li^+-TOP (−67.49 kcal/mol). It can be concluded that Li^+ is more inclined to bind to $[Tf_2N]^-$ in the extraction system, and the neutral ligand TOP coordinate with Li^+ to ensure the stability of the complex. This is consistent with the experimental results in Fig. 4, indicating that the IL plays a crucial role in the extraction process and only TOP cannot perform the extraction of Li^+. In addition, the stronger binding energy of Li^+-$[Tf_2N]^-$ than that of Li^+-$4H_2O$ indicates that the IL can effectively extract Li^+ from the aqueous phase. Fig. 8d–f show that there is the order of Mg^{2+}-$6H_2O$ (−337.41 kcal/mol) > Mg^{2+}-$[Tf_2N]^-$ (−337.27 kcal/mol) > Mg^{2+}-TOP (−177.46 kcal/mol) in the magnitude of interaction energies. This indicates that the very strong interaction presented between Mg^{2+} and H_2O lead to the

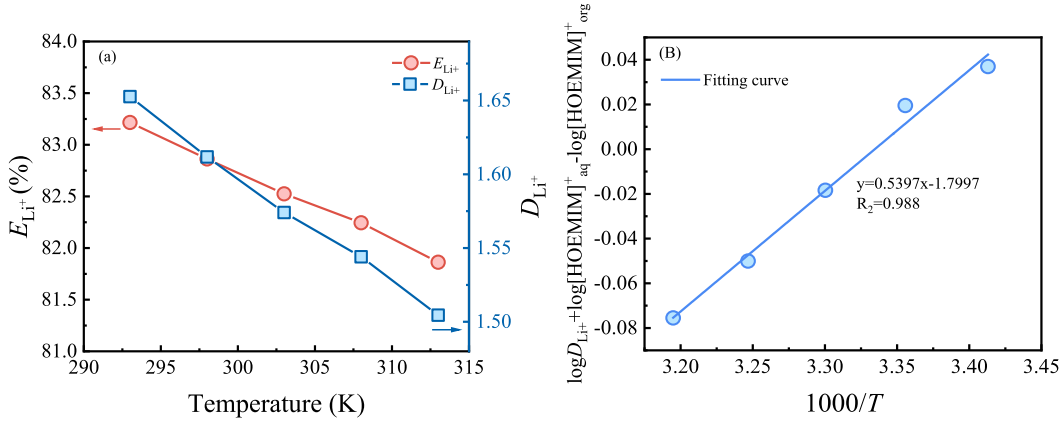

Fig. 7. Effect of temperature (a) and plot of versus 1000/T (b) for Li^+ extraction (O/A = 3:1 and pH = 7) at the normal atmosphere.

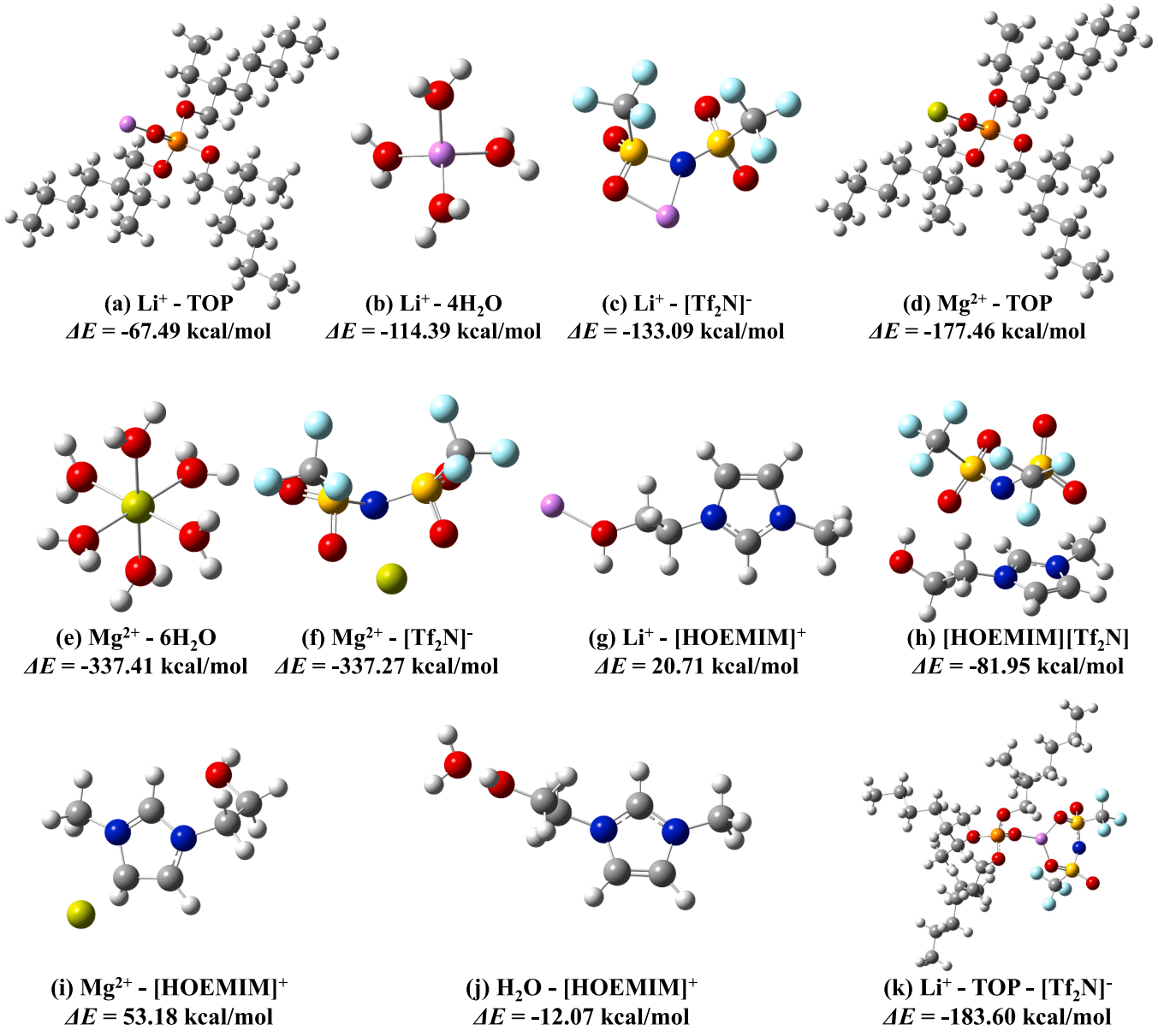

Fig. 8. Optimized structures and binding energy for clusters by QC calculations at B3LYP/6–31 + g(d,p) with DFT-D3(BJ) dispersion correction.

IL failed to effectively extract Mg^{2+}. This will cause to low extraction efficiency of Mg^{2+} and further increase the separation selectivity of Li^+/Mg^{2+}, which is also consistent with the experimental extraction results. In addition, it can be seen from by comparing Fig. 8d, f and h that the binding energy of $[HOEMIM]^+$-$[Tf_2N]^-$ (−81.95 kcal/mol) is the weakest, indicating that metal ions (Li^+ and Mg^{2+}) bind the anion $[Tf_2N]^-$ more competitively than the cation $[HOEMIM]^+$. Meanwhile, it can be found from Fig. 8g, i and j that the binding energy of Li^+-$[HOEMIM]^+$ and Mg^{2+}-$[HOEMIM]^+$ are positive, indicating that there is repulsive interaction presented between them. The negative binding energy of H_2O-$[HOEMIM]^+$ (−12.07 kcal/mol) can lead to the cation $[HOEMIM]^+$ entering the aqueous phase, while it can weaken the hydration of Li^+, and further promote transfer of Li^+ from the aqueous to organic phases. It can be seen from Fig. 8k that the binding energy of Li^+-TOP-$[Tf_2N]^-$ (−183.60 kcal/mol) is significantly stronger than those of Li^+-TOP (−67.49 kcal/mol) and Li^+-$[Tf_2N]^-$ (−133.09 kcal/mol), indicating that the TOP and anion $[Tf_2N]^-$ have the collaborative effect on extraction of Li^+.

4.5.2. Electrostatic potential (ESP) analysis

ESP is an effective method to determine the location and strength of possibly electrostatic interactions between molecules or clusters by analyzing the three-dimensional distribution map of ESP extreme points on the vdW surface of molecules. It can be seen from the Fig. 9a that the global minimum ESP point (−48.74 kcal/mol) of TOP was distributed near the O of P═O group, where will electrostatically interact with other molecules with positive ESP values. This is due to the oxygen atom have strong electronegativity due to the presence of lone-pair electrons, and the P═O group greatly enhanced the concentrated distribution of π-electron leading to the concentration of negative ESP points near the P═O group. Meanwhile, the dispersion of positive ESP points distributes around hydrogen atoms in the alkyl chain. Fig. 9b shows that the global minimum point of ESP (−114.38 kcal/mol) of $[Tf_2N]^-$ distributes near the oxygen atom, and the maximum point (−50.04 kcal/mol) appears above fluorine atoms. Notably, the global ESP minimum of $[Tf_2N]^-$ (−114.38 kcal/mol) is significantly more negative than that of TOP (−48.74 kcal/mol). As a result of the strong electrostatic attraction, Li^+ with a positive charge, preferably coordinates with the oxygen atom at the S═O group of $[Tf_2N]^-$, resulting in the formation of complex Li^+-

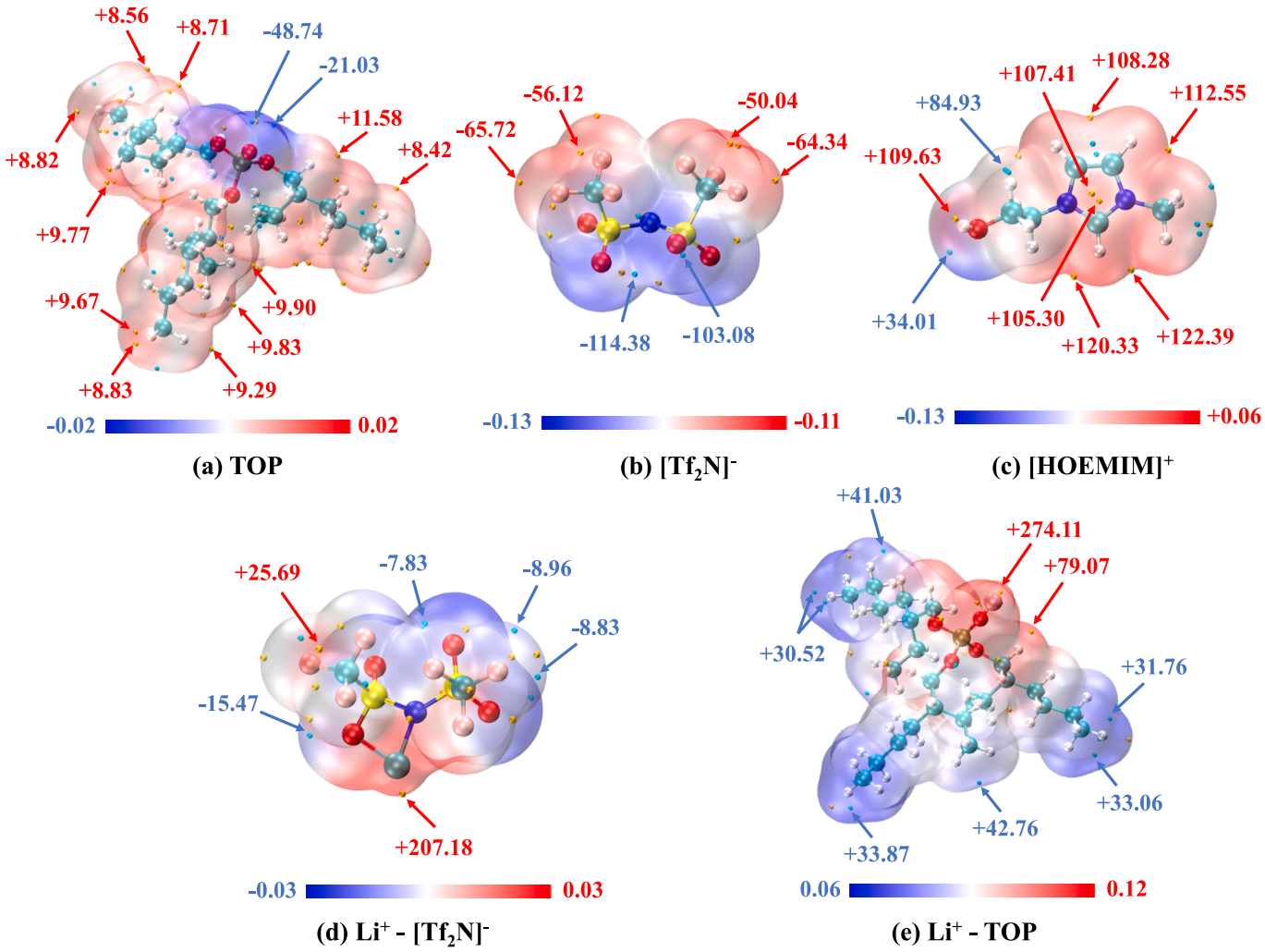

Fig. 9. ESP of molecular vdW surfaces of TOP, complex, cations and anions of ILs (The ESP maximum and minimum values are represented by yellow and cyan balls, respectively, units in kcal/mol). (For interpretation of the references to color in this figure legend, the reader is referred to the web version of this article.)

$[Tf_2N]^-$, as shown in Fig. 9d. The maximum ESP value of Li^+-$[Tf_2N]^-$ is concentrated near Li^+ (+207.18 kcal/mol). Due to the strong electronegativity of the oxygen atom on TOP, the O of the P═O group in TOP coordinates with Li^+, thereby forming Li^+-TOP complex as shown in Fig. 9E. In addition, the global maximum ESP point for Li^+-TOP appears near Li^+ (+274.11 kcal/mol), resulting in a strong electrostatic attraction between Li^+ and other molecule with negative ESP values like $[Tf_2N]^-$. Fig. 9c shows that the global ESP maximum point (+122.39 kcal/mol) for $[HOEMIM]^+$ is distributed around the acid hydrogen atom on the imidazolium ring of cation, which is significantly lower than that of Li^+-TOP (+274.11 kcal/mol). This interaction promotes cation exchange between Li^+ and $[HOEMIM]^+$, causing the transfer of Li^+ from the aqueous to organic phase by the strong electrostatic interaction between Li^+ and TOP/$[Tf_2N]^-$. These findings are consistent with the experimental, spectroscopic characterization and binding energy analyses.

4.5.3. *Independent gradient model (IGM) analysis*

IGM analysis as proposed by Lefebvre et al., can intuitively identify the size, type and location of noncovalent interactions between molecules, the IGM analyses regarding the molecular-level mechanism for extraction of Li^+ are shown in Fig. 10. As shown in Fig. 10a, a blue-green isosurface and coordination bond ($Li^+ \rightarrow$ O═P) appears between the Li^+ and oxygen atom of the P═O group, which is due to the coordination interaction between the oxygen atom containing lone pair electrons and Li^+ providing empty electron orbitals. Fig. 10b shows that there are four blue green isosurfaces presented between Li^+ and the oxygen atoms of the H_2O molecules, indicating the strong Li^+ hydration formed in the H-O···Li^+ bond similar to HBs. It can be found in Fig. 10c that there are two blue green isosurfaces located between Li^+ and the nitrogen with the oxygen of $[Tf_2N]^-$, respectively, indicating the electrostatic attraction between Li^+ and $[Tf_2N]$ in S-N···Li^+ and S═O···Li^+ interactions. Fig. 10d shows that there are two blue-green areas presented between Mg^{2+} and the oxygen atom on TOP with carbons alkyl chain, respectively. Compared with area of isosurface of Li^+-TOP, that of Mg^{2+}-TOP is bluer and larger, representing a stronger interaction formed in the latter. This is consistent with the binding energy and ESP analyses. As shown in Fig. 10e, a huge blue-green isosurface occupies almost all of the space between the Mg^{2+} and six H_2O molecules, which represents the very strong Mg^{2+} hydration formed in the H-O···Mg bonds and the its strength is obviously stronger than that of Li^+-4H_2O due to the larger area of isosurfaces in the former when compared with that in the latter (see Fig. 10b). Fig. 10f shows that the larger bule green area is resented in Mg^{2+}-$[Tf_2N]^-$ than that in Li^+-$[Tf_2N]^-$, indicating that the former has the stronger interaction than the latter. These findings are in the accordance with the binding energy and ESP analyses. Meanwhile, the Mg^{2+}-6H_2O complex has the larger area of isosurfaces than Mg^{2+}-TOP and Mg^{2+}-$[Tf_2N]^-$ complexes, indicating that the hydration interaction between Mg^{2+} and H_2O molecules is stronger than that between Mg^{2+} and TOP/IL. This validates that it is difficult to extract Mg^{2+} from the

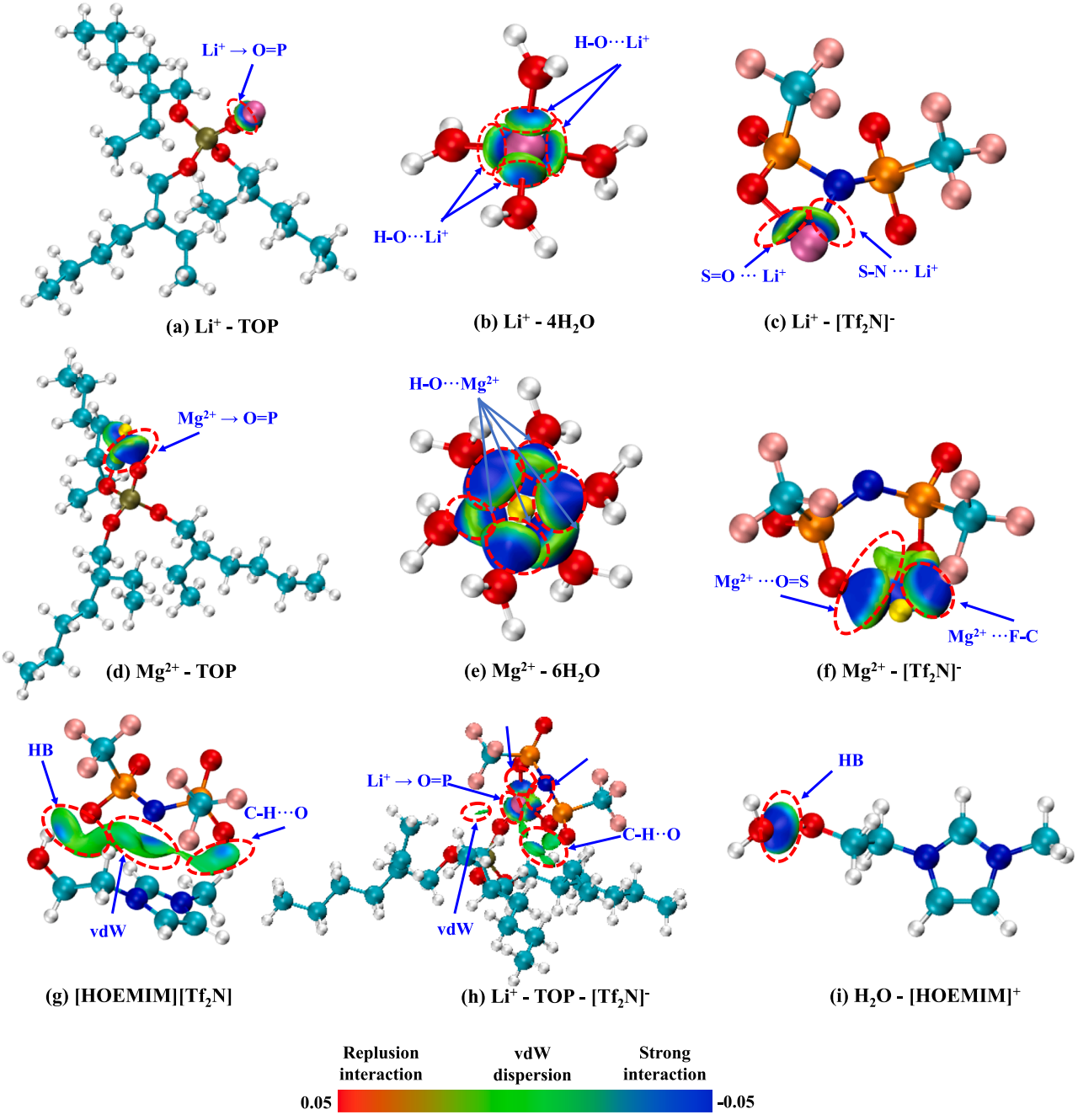

Fig. 10. IGM visualization for different complex. (The isovalue of IGM is 0.01, and the color scale is shown in ranging from −0.05 to 0.05 au).

aqueous to organic phases by using the extractant of IL + TOP, which further leads to the high separation selectivity for Li^+/Mg^{2+}. For [HOEMIM][Tf_2N], it is found in Fig. 10g that an isosurface is formed between oxygen atoms of $[Tf_2N]^-$ and the hydrogen atom on hydroxyl of $[HOEMIM]^+$, representing the formation of HB interaction of O-H···O. Similarly, hydrogen atoms on alky chain of $[HOEMIM]^+$ and oxygen atoms of $[Tf_2N]^-$ can form the electrostatic interaction of C-H···O and vdW dispersion. Fig. 10h shows that the electrostatic interaction of S═O···Li^+ can be formed between Li^+ and $[Tf_2N]^-$ except for the coordination interaction of Li^+ → O═P in the complex Li^+-TOP-$[Tf_2N]^-$. Moreover, C-H···O interactions can be also formed between the hydrogen atoms on alkyl chains of TOP and oxygen atoms of $[Tf_2N]^-$, and a thin green isosurface exists between the fluorine atom of $[Tf_2N]^-$ and hydrogen atoms of TOP, where the vdW dispersion is formed. Therefore, various interactions of Li^+ → O═P, S-N···Li^+, S═O···Li^+, C-H···O, and vdW dispersion are simultaneously existed in the complex of Li^+-TOP-$[Tf_2N]^-$ to form the so-called multi-site interaction, demonstrating that Li^+-TOP-$[Tf_2N]^-$ has stronger interaction than Li^+-TOP and Li^+-$[Tf_2N]^-$. This also confirm that both TOP and IL contribute to the extraction of Li^+, which is consistent with the experimental results of extraction equilibrium, that is, Li^+ is extracted from aqueous to organic phases by the way of the complex Li^+-TOP-[Tf_2N]. Fig. 10I shows that there is a bule isosurface presented between the hydrogen atom on hydroxyl of $[HOEMIM]^+$ and the oxygen atom of H_2O, representing the formation of HB (H-O··H) interaction, which can weaken the hydration of Li^+ in the aqueous phase and promote its exchange transfer into the organic phase. These above-mentioned findings are consistent with experimental extraction results, spectroscopic characterization, binding energy and ESP analyses. In short, Li^+ mainly interacts electrostatically with the anion $[Tf_2N]^-$ of IL in the form of S-N···Li^+ and S═O···Li^+. The

cation mainly undergoes HB interaction with H_2O and enters the aqueous phase undertaking ion exchange with Li^+, so that Li^+ in the aqueous phase enters the organic phase of IL + TOP through the Li^+-TOP-$[Tf_2N]^-$form of the complex. In this case, the coordinate interaction ($Li^+ \rightarrow O{=}P$,) can be formed between Li^+ and TOP, the electrostatic interactions (S-N···Li^+ and S═O···Li^+) can be formed Li^+-$[Tf_2N]^-$, as well the C-H···O and vdW interactions can be presented between TOP and $[Tf_2N]^-$. Therefore, the IL can act as a co-extractant as well as a stabilizing complex in an electrically neutral form during the Li^+ extraction process.

4.6. Washing and stripping experiment results

During the extraction Li^+ process, despite a high separation selectivity of Li^+/Mg^{2+}, a small amount of Mg^{2+} are still extracted into the Li^+-loaded organic phase. To remove these excess Mg^{2+} and obtain high-pure Li^+ organic phase for preparing the product containing Li^+, the washing experiment was conducted. According to the cation exchange theory, the binding order of TOP and metal ions is $H^+ > Li^+ > Na^+ > Mg^{2+}$ (Wang et al., 2018). Therefore, NaCl and LiCl selected as detergents to remove Mg^{2+} in the organic phase was investigated experimentally. As shown in Fig. 11a (see Tables S7 in Supplementary material for more details), the washing efficiencies of both Li^+ and Mg^{2+} rise with the increase in the NaCl concentration. When the NaCl concentration is 0.5 mol/L, the washing efficiency of Mg^{2+} reaches 99.29 %. In this case, the washing efficiency of Li^+ can also reach 45.71 %, which leads to the severe loss of Li^+. To overcome this problem, LiCl was also added to the detergent under the 0.5 mol/L NaCl, and the results are shown in the Fig. 11b (see Tables S8 in Supplementary material for more details). It is found that the washing efficiency of Li^+ significantly decreases with the increase in the LiCl concentration. Under the LiCl concentration of 0.1 mol/L, the washing efficiencies of Li^+ and Mg^{2+} in the organic phase after extraction are 1.77 % and 99.7 %, respectively, demonstrating the effectiveness of LiCl against washing Li^+. The Mg^{2+} concentration in the organic phase after washing is almost zero, and then the Li^+ and introduced Na^+ need to be stripped by HCl solution of 0.5 mol/L from the organic phase into the aqueous phase to facilitate the production of Li_2CO_3 subsequently. The experimental results are shown in Fig. 11c (see Table S9 in Supplementary material more details). When the ratio of O/A is 4:1, the Li^+ stripping rate is only 49.2 % due to the small amount of HCl aqueous solution leading to insufficient mass transfer. The stripping efficiency of Li^+ significantly increase with the increase in O/A ratio ranging from 4:1 to 2:1. When the O/A ratio over 2:1, the stripping efficiency of Li^+ is almost unchanged with increasing the O/A ratio, so the optimal O/A ratio of 1:1 is selected with the stripping efficiency of Li^+ of 99.90 %.

4.7. Recycling performance of extractant

The extractant-loaded organic phase is acidic after stripping experiment, so it is not suitable for repeated extraction of Li^+. Therefore, ammonia solution of 1 mol/L was used to neutralize the H^+ in the organic phase to regenerate the extractant. It can be seen from the Fig. 12a (see Tables S10 in Supplementary material for more details) that after 6 extractions with the regenerated extractant of IL + TOP, the extraction of Li^+ has not obvious decrease keep with around 80 %.

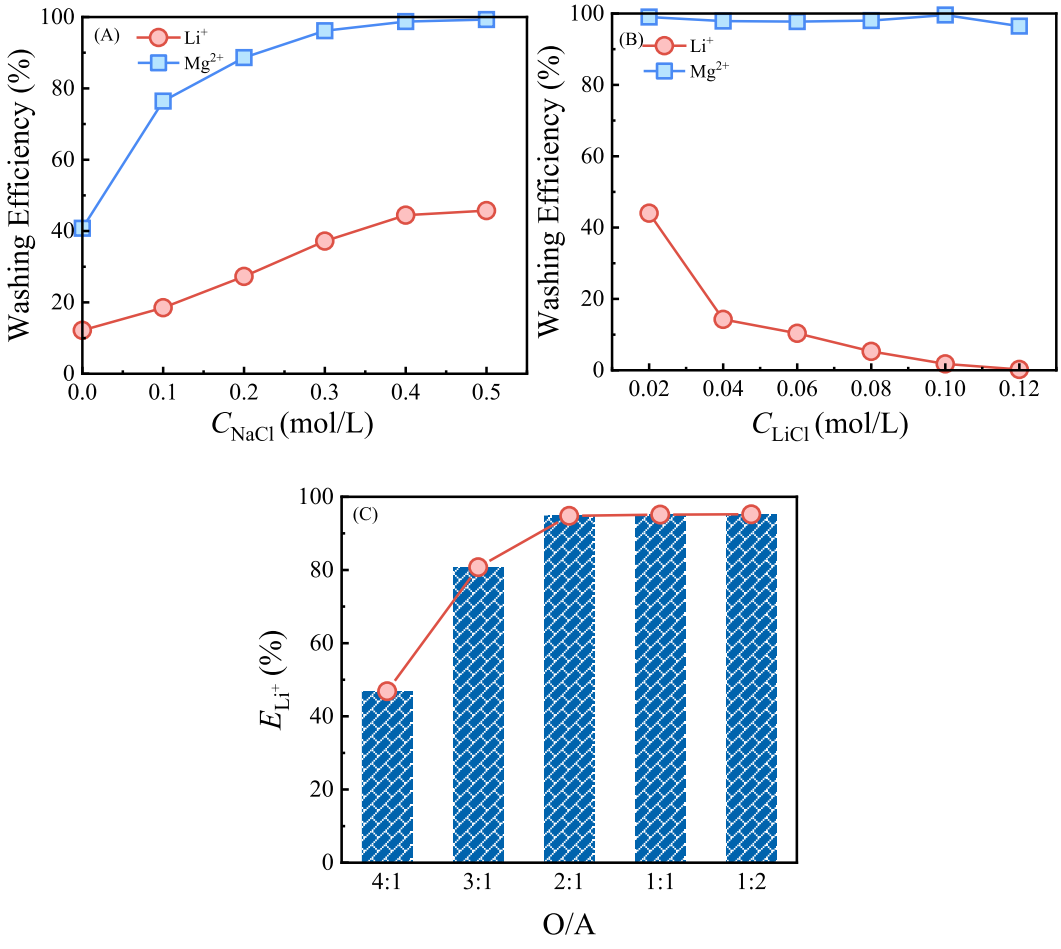

Fig. 11. Effects of NaCl (O/A = 3:1) (a) and LiCl (O/A = 3:1 and C_{NaCl} = 0.5 mol/L) (b) concentrations on washing efficiency of metal ions, and effects of different O/A ratios on the stripping efficiency of Li^+ (c) at 298.15 K.

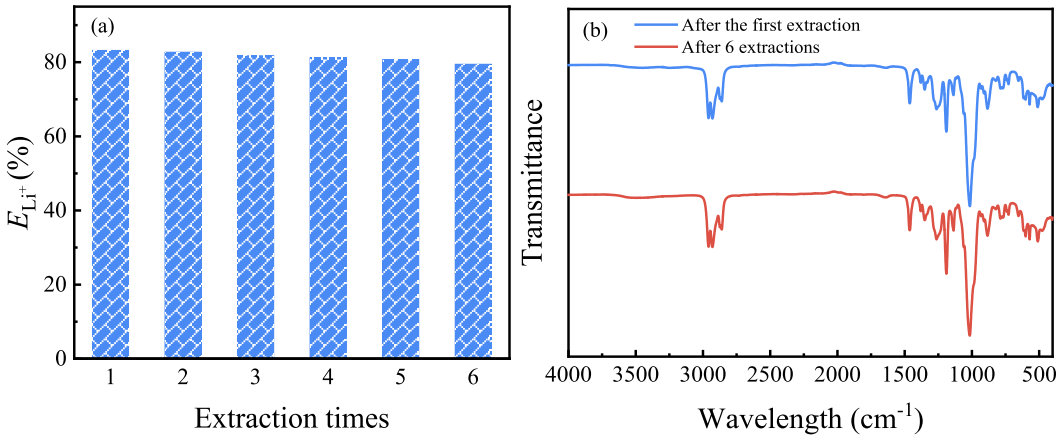

Fig. 12. The cycling extraction efficiency of Li^+ (a) and FTIR spectra of the regenerated extractant of [HOEMIM][Tf_2N] + TOP (b) at 298.15 K.

Fig. 12b shows that the FTIR spectra of extractant regenerated once and regenerated 6 times are the same, indicating that the collaborative extractant of IL + TOP has excellent regenerable and cycling extraction performance with the promising potential in the real industrial application.

5. Conclusions

In this work, we systematically investigated selective extraction of Li^+ with IL-based collaborative extractant from brines with high Mg^{2+}/Li^+ molar ratio. The [HOEMIM][Tf_2N] + TOP was selected as the best candidate with the extraction efficiency of Li^+ up to 83.16 % and separation selectivity of Li^+/Mg^{2+} up to 742.11 at the single-stage extraction, as well as the extraction efficiency of Li^+ up to 99.07 % at the five-stage extraction. It was found that Li^+ can be extracted from the aqueous to organic phases in the form of Li^+-TOP-[Tf_2N]$^-$ complex of 1:1:1 in molar ratio. The thermodynamic model ePC-SAFT was first extended to quantitatively predict the phase equilibria of the so-called "organic–inorganic complex strong electrolyte system" presented in this work, without adjusting additionally binary interaction parameters. The molecular-level extraction mechanisms were investigated by analyzing binding energies, ESP and IGM. The results showed that the Li^+ and Mg^{2+} were hydrated by strong interaction of "Metal-O-H", and the Li^+ hydration is weaker than Mg^{2+} hydration. The Li^+ can be extracted from the aqueous to organic phases by producing the complex of Li^+-TOP-[Tf_2N]$^-$ dominated by the multi-site interaction consisting of $Li^+ \rightarrow$ O═P, S-N···Li^+, S═O···Li^+ C-H···O, and vdW dispersion interactions together, which are stronger than Li^+ hydration energy. In this case, TOP plays an extractant by the coordinate interaction ($Li^+ \rightarrow$ O═P) and the IL plays a co-extractant as well as a stabilizing complex in an electrically neutral form. The collaborative extractant of [HOEMIM][Tf_2N] + TOP has the good recycling capacity without significant decrease for the extraction performance after six cycles. This work aims to provide theoretical guidance for rational design of a novel IL-based extractant for the high-efficiency extraction of Li^+ from high Mg^{2+}/Li^+ ratio brines.

CRediT authorship contribution statement

Gangqiang Yu: Conceptualization, Investigation, Methodology, Validation, Visualization, Writing – original draft. **Xinhe Zhang:** Data curation, Investigation, Methodology, Validation. **Tobias Hubach:** Conceptualization, Formal analysis, Investigation, Validation, Writing – original draft. **Biaohua Chen:** Conceptualization, Project administration, Supervision. **Christoph Held:** Conceptualization, Methodology, Resources, Software, Supervision, Investigation, Validation, Writing – review & editing.

Declaration of competing interest

The authors declare that they have no known competing financial interests or personal relationships that could have appeared to influence the work reported in this paper.

Data availability

Data will be made available on request.

Acknowledgments

This work was financially supported by the National Natural Science Foundation of China under Grants (Nos. 22378006 and 22008003). The authors acknowledge funding from the Alexander von Humboldt Foundation (G. Yu). We acknowledge financial support realized through the DEAL contract with Elsevier.

Appendix A. Supplementary data

Supplementary data to this article can be found online at https://doi.org/10.1016/j.ces.2023.119682.

References

Andeen, C., Fontanella, J., Schuele, D., 1970. Low-frequency dielectric constant of LiF, NaF, NaCl, NaBr, KCl, and KBr by the method of substitution. Phys. Rev. B 2, 5068.
Andersson, M.P., Uvdal, A., 2005. New scale factors for harmonic vibrational frequencies using the B3LYP density functional method with the triple-ζ basis set 6–311+G(d, p). J. Phys. Chem. A 109, 2937–2941.
Ascani, M., Held, C., 2021. Prediction of salting-out in liquid-liquid two-phase systems with ePC-SAFT: Effect of the Born term and of a concentration-dependent dielectric constant. Z. Anorg. Allg. Chem. 647, 1305–1314.
Ascani, M., Sadowski, G., Held, C., 2022. Calculation of multiphase equilibria containing mixed solvents and mixed electrolytes: general formulation and case studies. J. Chem. Eng. Data 67, 1972–1984.
Berthelot, D., 1898. Sur le mélange des gaz. Compt. Rendus. 126, 15.
Bülow, M., Ji, X., Held, C., 2019. Incorporating a concentration-dependent dielectric constant into ePC-SAFT. An application to binary mixtures containing ionic liquids. Fluid Phase Equilib. 492, 26–33.
Bülow, M., Ascani, M., Held, C., 2021a. ePC-SAFT advanced – Part I: Physical meaning of including a concentration-dependent dielectric constant in the born term and in the Debye-Hückel theory. Fluid Phase Equilib. 535, 112967.
Bülow, M., Ascani, M., Held, C., 2021b. ePC-SAFT advanced – Part II: Application to salt solubility in ionic and organic solvents and the impact of ion pairing. Fluid Phase Equilib. 537, 112989.
Cai, C., Hanada, T., Fajar, A.T.N., Goto, M., 2021. An ionic liquid extractant dissolved in an ionic liquid diluent for selective extraction of Li(I) from salt lakes. Desalination 509.
Cameretti, L.F., Sadowski, G., 2008. Modeling of aqueous amino acid and polypeptide solutions with PC-SAFT. Chem. Eng. Process. Process Intensification 47, 1018–1025.

Cameretti, L.F., Sadowski, G., Mollerup, J.M., 2005. Modeling of aqueous electrolyte solutions with perturbed-chain statistical associated fluid theory. Ind. Eng. Chem. Res. 44, 3355–3362.
Chapeaux, A., Simoni, L.D., Stadtherr, M.A., Brennecke, J.F., 2007. Liquid phase behavior of ionic liquids with water and 1-octanol and modeling of 1-octanol/water partition coefficients. J. Chem. Eng. Data 52, 2462–2467.
Chen, X., Yuan, S., Abdeltawab, A.A., Al-Deyab, S.S., Zhang, J., Yu, L., Yu, G., 2014. Extractive desulfurization and denitrogenation of fuels using functional acidic ionic liquids. Sep. Purif. Technol. 133, 187–193.
Chen, L., Zhou, T., Chen, L., Ye, Y., Qi, Z., Freund, H., Sundmacher, K., 2011. Selective oxidation of cyclohexanol to cyclohexanone in the ionic liquid 1-octyl-3-methylimidazolium chloride. Chem. Comm. 47, 9354–9356.
Chen, L., Zhang, T., Cheng, H., Richards, R.M., Qi, Z., 2020. A microwave assisted ionic liquid route to prepare bivalent Mn 5 O 8 nanoplates for 5-hydroxymethylfurfural oxidation. Nanoscale 12, 17902–17914.
Choubey, P.K., Kim, M.-S., Srivastava, R.R., Lee, J.-C., Lee, J.-Y., 2016. Advance review on the exploitation of the prominent energy-storage element: Lithium. Part I: From mineral and brine resources. Miner. Eng. 89, 119–137.
Cui, L., Jiang, K., Wang, J., Dong, K., Zhang, X., Cheng, F., 2019. Role of ionic liquids in the efficient transfer of lithium by Cyanex 923 in solvent extraction system. AIChE J. 65, e16606.
Cui, L., Li, S., Kang, J., Yin, C., Guo, Y., He, H., Cheng, F., 2021. A novel ion-pair strategy for efficient separation of lithium isotopes using crown ethers. Sep. Purif. Technol. 274, 118989.
Dupont, D., Binnemans, K., 2015. Rare-earth recycling using a functionalized ionic liquid for the selective dissolution and revalorization of Y 2 O 3: Eu 3+ from lamp phosphor waste. Green Chem. 17, 856–868.
Frisch, M., Trucks, G., Schlegel, H., Scuseria, G., Robb, M., Cheeseman, J., Scalmani, G., Barone, V., Mennucci, B., Petersson, G., 2009. Gaussian 09 (Revision D.01).
Gao, D., Yu, X., Guo, Y., Wang, S., Liu, M., Deng, T., Chen, Y., Belzile, N., 2015. Extraction of lithium from salt lake brine with triisobutyl phosphate in ionic liquid and kerosene. Chem. Res. Chin. Univ. 31, 621–626.
Grimme, S., Ehrlich, S., Goerigk, L., 2011. Effect of the damping function in dispersion corrected density functional theory. J. Comput. Chem. 32, 1456–1465.
Gross, J., Sadowski, G., 2001. Perturbed-chain SAFT: An equation of state based on a perturbation theory for chain molecules. Ind. Eng. Chem. Res. 40, 1244–1260.
Gu, D., Sun, W., Han, G., Cui, Q., Wang, H., 2018. Lithium ion sieve synthesized via an improved solid state method and adsorption performance for West Taijinar Salt Lake brine. Chem. Eng. J. 350, 474–483.
Held, C., Cameretti, L.F., Sadowski, G., 2008. Modeling aqueous electrolyte solutions: Part 1. Fully dissociated electrolytes. Fluid Phase Equilib. 270, 87–96.
Held, C., Reschke, T., Mohammad, S., Luza, A., Sadowski, G., 2014. ePC-SAFT revised. Chemical Eng. Res. Des. 92, 2884–2897.
Jiang, C., Cheng, H., Qin, Z., Wang, R., Chen, L., Yang, C., Qi, Z., Liu, X., 2021. COSMO-RS prediction and experimental verification of 1, 5-pentanediamine extraction from aqueous solution by ionic liquids. Green Energy Environ. 6, 422–431.
Jin, W., Hu, M., Sun, Z., Huang, C.-H., Zhao, H., 2021. Simultaneous and precise recovery of lithium and boron from salt lake brine by capacitive deionization with oxygen vacancy-rich CoP/Co3O4-graphene aerogel. Chem. Eng. J. 420, 127661.
Keller, A., Hlawitschka, M., Bart, H.-J., 2021. Manganese recycling of spent lithium-ion batteries via solvent extraction. Sep. Purif. Technol. 275, 119166.
Kesler, S.E., Gruber, P.W., Medina, P.A., Keoleian, G.A., Everson, M.P., Wallington, T.J., 2012. Global lithium resources: Relative importance of pegmatite, brine and other deposits. Ore. Geol. Rev. 48, 55–69.
Kuang, G., Liu, Y., Li, H., Xing, S., Li, F., Guo, H., 2018. Extraction of lithium from β-spodumene using sodium sulfate solution. Hydrometallurgy 177, 49–56.
Lei, Z., Dai, C., Zhu, J., Chen, B., 2014. Extractive distillation with ionic liquids: a review. AIChE J. 60, 3312–3329.
Li, Z., Binnemans, K., 2020. Selective removal of magnesium from lithium-rich brine for lithium purification by synergic solvent extraction using β-diketones and Cyanex 923. AIChE J. 66, e16246.
Li, Z., Binnemans, K., 2021. Opposite selectivities of tri- n -butyl phosphate and Cyanex 923 in solvent extraction of lithium and magnesium. AIChE J. 67, e17219.
Li, Z., Mercken, J., Li, X., Riaño, S., Binnemans, K., 2019b. Efficient and sustainable removal of magnesium from brines for lithium/magnesium separation using binary extractants. ACS Sustainable Chem. Eng. 7, 19225–19234.
Li, Z., Zhang, Z., Onghena, B., Li, X., Binnemans, K., 2021. Ethylammonium nitrate enhances the extraction of transition metal nitrates by tri-n-butyl phosphate (TBP). AIChE J. 67, e17213.
Li, Y.-H., Zhao, Z.-W., Liu, X.-H., Chen, X.-Y., Zhong, M.-L., 2015. Extraction of lithium from salt lake brine by aluminum-based alloys. Trans. Nonferrous. Met. Soc. China 25, 3484–3489.
Li, Y., Zhao, Y., Wang, H., Wang, M., 2019a. The application of nanofiltration membrane for recovering lithium from salt lake brine. Desalination 468.
Liu, X., Zhong, M., Chen, X., Zhao, Z., 2018. Separating lithium and magnesium in brine by aluminum-based materials. Hydrometallurgy 176, 73–77.
Lorentz, H.A., 1881. Ueber die Anwendung des Satzes vom Virial in der kinetischen Theorie der Gase. Ann. Phys. 248, 127–136.
Lu, T., Chen, F., 2012. Multiwfn: a multifunctional wavefunction analyzer. J. Comput. Chem. 33, 580–592.
Marcus, Y., 1988. Ionic radii in aqueous solutions. Chem. Rev. 88, 1475–1498.
Navarro, P., Moreno, D., Larriba, M., García, J., Rodríguez, F., Canales, R.I., Palomar, J., 2023. An overview process analysis of the aromatic-aliphatic separation by liquid-liquid extraction with ionic liquids. Sep. Purif. Technol. 316, 123848.
Olsher, U., Izatt, R.M., Bradshaw, J.S., Dalley, N.K., 1991. Coordination chemistry of lithium ion: a crystal and molecular structure review. Chemical Reviews 91, 137–164.
Pramanik, B.K., Nghiem, L.D., Hai, F.I., 2020. Extraction of strategically important elements from brines: Constraints and opportunities. Water Res. 168, 115149.
Qin, L., Zhang, J., Cheng, H., Chen, L., Qi, Z., Yuan, W., 2016. Selection of imidazolium-based ionic liquids for vitamin E extraction from deodorizer distillate. ACS Sustainable Chem. Eng. 4, 583–590.
Rout, A., Binnemans, K., 2015. Influence of the ionic liquid cation on the solvent extraction of trivalent rare-earth ions by mixtures of Cyanex 923 and ionic liquids. Dalton. Trans. 44, 1379–1387.
Shi, D., Cui, B., Li, L., Peng, X., Zhang, L., Zhang, Y., 2019. Lithium extraction from low-grade salt lake brine with ultrahigh Mg/Li ratio using TBP – kerosene – $FeCl_3$ system. Sep. Purif. Technol. 211, 303–309.
Shi, D., Cui, B., Li, L., Xu, M., Zhang, Y., Peng, X., Zhang, L., Song, F., Ji, L., 2020. Removal of calcium and magnesium from lithium concentrated solution by solvent extraction method using D2EHPA. Desalination 479, 114306.
Shi, C., Duan, D., Jia, Y., Jing, Y., 2014. A highly efficient solvent system containing ionic liquid in tributyl phosphate for lithium ion extraction. J. Mol. Liq. 200, 191–195.
Shi, C., Jing, Y., Jia, Y., 2016. Solvent extraction of lithium ions by tri-n-butyl phosphate using a room temperature ionic liquid. J. Mol. Liq. 215, 640–646.
Shi, C., Jing, Y., Xiao, J., Wang, X., Yao, Y., Jia, Y., 2017. Solvent extraction of lithium from aqueous solution using non-fluorinated functionalized ionic liquids as extraction agents. Sep. Purif. Technol. 172, 473–479.
Shi, D., Zhang, L., Peng, X., Li, L., Song, F., Nie, F., Ji, L., Zhang, Y., 2018. Extraction of lithium from salt lake brine containing boron using multistage centrifuge extractors. Desalination 441, 44–51.
Song, Z., Zhou, T., Zhang, J., Cheng, H., Chen, L., Qi, Z., 2015. Screening of ionic liquids for solvent-sensitive extraction–with deep desulfurization as an example. Chem. Eng. Sci. 129, 69–77.
Song, Z., Zeng, Q., Zhang, J., Cheng, H., Chen, L., Qi, Z., 2016. Solubility of imidazolium-based ionic liquids in model fuel hydrocarbons: A COSMO-RS and experimental study. J. Mol. Liq. 224, 544–550.
Su, H., Li, Z., Zhang, J., Liu, W., Zhu, Z., Wang, L., Qi, T., 2020. Combining selective extraction and easy stripping of lithium using a ternary synergistic solvent extraction system through regulation of Fe3+ coordination. ACS Sustainable Chem. Eng. 8, 1971–1979.
Su, H., Tan, B., Zhang, J., Liu, W., Wang, L., Wang, Y., Zhu, Z., Qi, T., 2022. Modelling of lithium extraction with TBP/P507–FeCl3 system from salt-lake brine. Sep. Purif. Technol. 282, 120110.
Sun, X., Wang, X., Wan, Y., Guo, Y., Deng, T., Yu, X., 2023. Synthesis of functional ionic liquids with high extraction rate and electroconductivity for lithium-magnesium separation and metallic magnesium production from salt lake brine. Chem. Eng. J. 452, 139610.
Tarascon, J.-M., 2010. Is lithium the new gold? Nature Chem. 2, 510.
Wang, K., Adidharma, H., Radosz, M., Wan, P., Xu, X., Russell, C.K., Tian, H., Fan, M., Yu, J., 2017. Recovery of rare earth elements with ionic liquids. Green Chem. 19, 4469–4493.
Wang, Y., Liu, H., Fan, J., Liu, X., Hu, Y., Hu, Y., Zhou, Z., Ren, Z., 2018. Recovery of lithium ions from salt lake brine with a high magnesium/lithium ratio using heteropolyacid ionic liquid. ACS Sustainable Chem. Eng. 7, 3062–3072.
Wang, Y., Duan, W., Li, R., Zhang, F., Tian, S., Ren, Z., Zhou, Z., 2023. One-step synthesis of heteropolyacid ionic liquid as co-extraction agent for recovery of lithium from aqueous solution with high magnesium/lithium ratio. Desalination 548.
Wang, J., Yang, S., Bai, R., Chen, Y., Zhang, S., 2019. Lithium recovery from the mother liquor obtained in the process of Li2CO3 production. Ind. Eng. Chem. Res. 58, 1363–1372.
Weil, M., Ziemann, S., Schebek, L., 2009. How to assess the availability of resources for new technologies? Case study: lithium a strategic metal for emerging technologies. Metall. Res. Technol. 106, 554–558.
Wolbach, J.P., Sandler, S.I., 1997. Using molecular orbital calculations to describe the phase behavior of hydrogen-bonding fluids. Ind. Eng. Chem. Res. 36, 4041–4051.
Xu, S., Song, J., Bi, Q., Chen, Q., Zhang, W.-M., Qian, Z., Zhang, L., Xu, S., Tang, N., He, T., 2021. Extraction of lithium from Chinese salt-lake brines by membranes: Design and practice. J Membr Sci. 635, 119441.
Yu, X., Cui, J., Liu, C., Yuan, F., Guo, Y., Deng, T., 2021b. Separation of magnesium from high Mg/Li ratio brine by extraction with an organic system containing ionic liquid. Chem. Eng. Sci. 229, 116019.
Yu, G., Sui, X., Lei, Z., Dai, C., Chen, B., 2019a. Air-drying with ionic liquids. AIChE J. 65, 479–482.
Yu, G., Mu, M., Li, J., Wu, B., Xu, R., Liu, N., Chen, B., Dai, C., 2020. Imidazolium-based ionic liquids introduced into π-electron donors: highly efficient toluene capture. ACS Sustainable Chem. Eng. 8, 9058–9069.
Yu, G., Dai, C., Wu, B., Liu, N., Chen, B., Xu, R., 2021a. Chlorine drying with hygroscopic ionic liquids. Green Energy Environ. 6, 350–362.
Yu, X., Fan, X., Guo, Y., Deng, T., 2019b. Recovery of lithium from underground brine by multistage centrifugal extraction using tri-isobutyl phosphate. Sep. Purif. Technol. 211, 790–798.

Yu, G., Gajardo-Parra, N.F., Chen, M., Chen, B., Sadowski, G., Held, C., 2023. Aromatic volatile organic compounds absorption with phenyl-based deep eutectic solvents: A molecular thermodynamics and dynamics study. AIChE J. 69, e18053.
Zhang, L., Li, L., Shi, D., Peng, X., Song, F., Nie, F., Han, W., 2018. Recovery of lithium from alkaline brine by solvent extraction with β-diketone. Hydrometallurgy 175, 35–42.
Zhang, J., Liu, Y., Liu, W., Wang, L., Chen, J., Zhu, Z., Qi, T., 2021. Mechanism study on the synergistic effect and emulsification formation of phosphine oxide with β-diketone for lithium extraction from alkaline systems. Sep. Purif. Technol. 279, 119648.
Zhao, A., Liu, J., Ai, X., Yang, H., Cao, Y., 2019. Highly selective and pollution-free electrochemical extraction of lithium by a polyaniline/Lix Mn2 O4 cell. ChemSusChem 12, 1361–1367.
Zhao, Z., Si, X., Liu, X., He, L., Liang, X., 2013. Li extraction from high Mg/Li ratio brine with $LiFePO_4/FePO_4$ as electrode materials. Hydrometallurgy 133, 75–83.
Zheng, H., Dong, T., Sha, Y., Jiang, D., Zhang, H., Zhang, S., 2021. Selective extraction of lithium from spent lithium batteries by functional ionic liquid. ACS Sustainable Chem. Eng. 9, 7022–7029.
Zhou, W., Li, Z., Xu, S., 2021. Extraction of lithium from magnesium-rich solution using tri-n-butyl phosphate and sodium hexafluorophosphate. J. Sustain. Metall. 7, 1368–1378.
Zhou, Z., Qin, W., Liang, S., Tan, Y., Fei, W., 2012. Recovery of lithium using tributyl phosphate in methyl isobutyl ketone and FeCl3. Ind. Eng. Chem. Res. 51, 12926–12932.
Zhou, Z., Liu, H., Fan, J., Liu, X., Hu, Y., Hu, Y., Wang, Y., Ren, Z., 2019. Selective extraction of lithium ion from aqueous solution with sodium phosphomolybdate as a coextraction agent. ACS Sustainable Chem. Eng. 7, 8885–8892.